Drones tracking based on robust Cubature Kalman-TBD-Multi-Bernoulli filter

Article *in* ISA Transactions · December 2020

DOI: 10.1016/j.isatra.2020.12.042

2 authors, including:

Mohamed Barbary
Nanjing University of Aeronautics and Astronautics
34 PUBLICATIONS **198** CITATIONS

ISA Transactions 114 (2021) 277–290

Contents lists available at ScienceDirect

ISA Transactions

journal homepage: www.elsevier.com/locate/isatrans

Research article

Drones tracking based on robust Cubature Kalman-TBD-Multi-Bernoulli filter

Mohamed Barbary [a,c,*], Mohamed H. Abd ElAzeem [b]

[a] Department of Electrical Engineering, Alexandria University, Alexandria, Egypt
[b] Department of electronics and communication, Arab Academy for Science Technology and Maritime Transport, Egypt
[c] Technical Research and Developing Centre, Elsayeda Aisha, Cairo, Egypt

ARTICLE INFO

Article history:
Received 23 August 2019
Received in revised form 19 December 2020
Accepted 23 December 2020
Available online 28 December 2020

Keywords:
Cubature Kalman Multi-Bernoulli Filter
Micro-drones tracking
Approximated variational Bayesian
TBD

ABSTRACT

The problem of nonlinear tracking and detection of small unmanned aerial vehicles and micro-drone targets is very challenging and has received great attention recently. Recently, the Cubature Kalman-multi-Bernoulli filter which employs a third-degree spherical-radical cubature rule has been presented to handle the nonlinear models. The Cubature Kalman filter is more principled and accurate in mathematical terms. In addition, a recent multi-Bernoulli filter based on variational Bayesian approximation has been presented with the estimation the fluctuation of variances of measurement. However, Cubature Kalman and variational Bayesian-Multi-Bernoulli filters are unsuitable for tracking the micro-drones because of the unknown probability of detection. As we known, the track-before-detect (TBD) schemes was an effective method for tracking the small objects. In this work, a novel robust Cubature Kalman-Multi-Bernoulli filter with variational Bayesian-TBD is proposed jointing with estimate the fluctuated variances of measurement. The improved filter is an effective method to solve the problem of detection profile estimation for micro-drones. A novel implementation with a non-linear Cubature Kalman Gaussian mixture and Inverse Gamma approximation is presented to estimate a hybrid kinematic state of micro-drones. The simulation results confirm the effectiveness and robustness of the proposed algorithm.

1. Introduction

This paper derives and demonstrates a random finite set (RFS)-based solution to tracking small unmanned aerial vehicles (UAVs) and micro-drones using the recently multi target multi-Bernoulli filter. The multi-Bernoulli filter has a good performance for tracking multi-target [1–4]. This filter has the posterior density for multi-target with direct propagate approximation. The most advantage of this filter has extracted the inexpensive and reliable state estimates. The multi-Bernoulli filter has a good performance with a known detection profile; otherwise, this filter will decrease the performance of tracking greatly.

The traditional tracking algorithm depends on the measurement parameters like range, speed and so forth. These measurement parameters extracted by the thresholding process. The main function of thresholding process is to reduce the data flow. For a given signal-to-noise ratio (SNR), the threshold determines probability of detection, and false alarm. In addition, the probability of false alarm affects the complexity of data association problem. Normally, a higher false alarm density needs more modified data association filters. These filters use a threshold level to extracting the exceeding cells. it is acceptable with a high SNR.

The improvement of traditional radar systems for tracking micro-drones has a seriously importance for more security. This is often challenging with small radar cross-section (RCS). Also, it flies at a low height and moves at low speed comparing to conventional objects such as aircraft, larger drones, helicopters and for applications of military [5]. For low SNR targets, the threshold must be smaller than the sufficient probability to avoid a high rate of false detection. Recent developments of detecting small targets have been presented to unknown probability of detection and fluctuation of RCS [5–10]. For small targets like drones, there is a substantial advantage of unthresholded approach jointing with tracking and detection, which known by track-before-detect (TBD). The multi-target tracking methods such as multiple model (MM) Bernoulli filters [11,12], and particle filter (PF) methods [13] have been presented for low SNR with some known parameters. But, all of them have an equivalent problem of slow adaptation to variances of the measurement with a heavy computation.

Since the variances of measurement are fluctuated in a real tracking scenario for small targets like drones. In [14,15], the multi-Bernoulli-TBD algorithms have been presented with a particle implementation and unknown probability of detection. But,

* Corresponding author.
E-mail address: mbarbary300@gmail.com (M. Barbary).

https://doi.org/10.1016/j.isatra.2020.12.042
0019-0578/

these methods aim at constant value of variances of measurement. Thus, they are unsuitable for small objects tracking. Recently, probability hypothesis density and multi-Bernoulli filters applied with approximated variational Bayesian method [16–20]. These algorithms are presented for a linear Gaussian implementation to estimate the variances of measurement. The approximation of hybrid posterior of the variances of measurement and states is done by factorizing a recursive expression and a fixed distribution. But, these algorithms aim at a constant value of probability of detection. Thus, they are unsuitable for tracking drones from image observations. The priori knowledge of critical parameter like a probability of detection is importance to enhance the filtering process. In addition, the probability of detection is not known a priori because of the fluctuation of small RCS. Thus, we propose a robust approximated variational Bayesian algorithm hybrid with TBD approach and multi-Bernoulli filter. It causes less computational burden instead of using variational Bayesian multi-Bernoulli and multi-Bernoulli-TBD filters. Further, we present a new solution for tracking drones includes the nonlinear implementation with unknown probability of detection and variances of measurement. Recently the Cubature Kalman filter which employs a third-degree spherical-radical cubature rule was proposed to handle the nonlinear models [21–23]. Compared with the particle filter, the Cubature Kalman filter is more accurate and more principled in mathematical terms. Therefore, in this paper, we study the joint usage of the Cubature Kalman approximation together with the variational Bayesian-multi-Bernoulli-TBD filter. The proposed algorithm introduces to hand the nonlinear filtering problem of drones.

The contributions of this work are summarized as:

- The multi-Bernoulli-TBD filter with sequential Monte Carlo (SMC) implementation has been used to the nonlinear tracking for small target with good performance. However, this implementation has the problem of slow adaptation to variances of the measurement with a heavy computation. This kind of algorithm brings amounts of computation burden and causes the overestimation of the number of target. Therefore, this filter is not accurate. In addition to, the filtering accuracy of the SMC-multi-Bernoulli-TBD filter is the worst because of the small particles number for each tracks. This filter is the optimal nonlinear multi-Bernoulli-TBD filtering approach. When the number of the particles for each tracks is large enough, this approach will get the best filtering accuracy. This may limit the real-time performance of the Multi-Bernoulli-TBD filtering.
- To solve this problem, we proposed a novel Cubature Kalman-multi-Bernoulli-TBD filter. The proposed algorithm employs a third-degree spherical-radical cubature rule. This filter is more accurate rather than the SMC-multi-Bernoulli-TBD filter and more principled in mathematical terms. This is the first time to use this Cubature Kalman-multi-Bernoulli filter for TBD approach. However, the proposed algorithm has implemented with fixed and known variances of measurement. Since the variances of measurement are unknown in a real tracking scenario for small targets like drones.
- To solve the problem of unknown variances of measurement due to the fluctuation of RCS. We improve the proposed algorithm to be suitable for tracking small objects with unknown variances of measurement. This improvement has applied with the approximated variational Bayesian approach to update the object state with unknown variances of measurement. This is the first time to use the proof of concept of this robust method for Cubature Kalman-multi-Bernoulli filter and TBD approach. Therefore, we propose a robust approximated variational Bayesian jointing with Cubature Kalman-multi-Bernoulli-TBD filter. The proposed algorithm has less computational burden comparing to SMC-multi-Bernoulli-TBD filter.

In Section 2 we explain a problem formulation, and in Section 3 we proposed a novel Cubature Kalman-variational Bayesian-multi-Bernoulli-TBD filter. The non-linear implementation of Cubature Kalman Gaussian and Inverse Gamma approximation is discussed in Section 4. Merging and pruning is presented in Section 5 and the simulations and results are presented in Section 6. Section 7 contains discussion and conclusions.

2. Problem of tracking micro-drones

The tracking techniques can be classified as classical radar tracking and Track-Before-Detect (TBD) approaches [24,25]. In the classical radar tracking, the radar video data is processed by applying a threshold, clustering and extraction, to obtain plots, in turn used for tracking algorithm [25]. The target detection involves thresholding at three stages. The first one is a signal strength thresholding on hit level is known by pre-detection stage. The second is a thresholding after binary integration of plot level is known by cluster and extraction stages. The third is a thresholding after binary integration on track level is known by tracking stage. The hard decision is made at the beginning of the process with respect to the presence of a possible target. As shown in Fig. 1, we can see that the thresholding is done directly on the radar video data for each scan. Data association and filtering are done after detection for final track output for each scan. In the classical method a low observable target such as drones does not always lead to a detection at each scan. When there is no detection no plots of the low observable target can be constructed and therefore this target will be declared lost. To overcome this problem, the Track-Before-Detect, so-called TBD approach is presented in this paper.

2.1. Track-before-detect (TBD) approach

The track-before-detect (TBD) method is an effective approach with a hybrid tracking and detection for the micro-drones with low SNR. The TBD approach proposes based the tracking on the raw video data instead of plots and thus avoid explicit data association step. Therefore, the traditional 3-stages threshold is replaced by a one stage including only the signal strength thresholding on track level by delaying the threshold. This delaying allowing the low observable target to build up, this achieves an improvement in the detection probability comparing to the classical method which using an equal false alarm probability. In TBD schemes the decision is processed the end of the DSP after all data from the radar which uses and integrates over the time. As shown in Fig. 1, this approach combines tracking and detection so that detection and track confirmation occur simultaneously. Therefore, the target detection and the states' estimation are an inseparable part of the same decision process.

2.2. Drones tracking model based on TBD approach

Let us consider at time k, there are $\mathcal{M}(k)$ drones states $\boldsymbol{x}_{k,1}, \ldots, \boldsymbol{x}_{k,\mathcal{M}(k)}$ in a matrix $\mathcal{S}$, the nonlinear dynamic model of target ℓ described by:

$$\boldsymbol{x}_{k,\ell} = \Phi_k\left(\boldsymbol{x}_{k-1,\ell}, w_k\right), \ell = 1, 2, \ldots, \mathcal{M}(k) \quad (1)$$

where $\boldsymbol{x}_{k,\ell} = \left[x_{k,\ell}\dot{x}_{k,\ell}y_{k,\ell}\dot{y}_{k,\ell}I_{k,\ell}\right]^T$ is the nonlinear state of target ℓ which contains the position, range rate and amplitude at instant k, Φ_k is known nonlinear function of $\boldsymbol{x}_{k,\ell}$ and w_k is a Gaussian

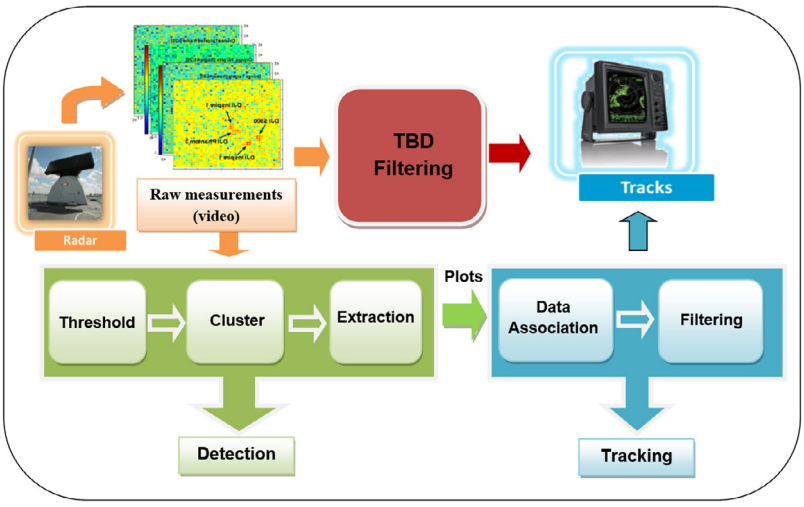

Fig. 1. Track-before-detect (TBD) and classical radar signal processing.

noise. Under the random finite set (RFS) framework, the multi-target state set $\boldsymbol{X}_k$ are finite sets, $\boldsymbol{X}_k = \left\{\boldsymbol{x}_{k,1}, \ldots, \boldsymbol{x}_{k,\mathcal{M}(k)}\right\} \subset \mathcal{S}$, $\mathcal{S} = \mathbb{R}^n$. Let us consider at time k, the observation model related to the RCS fluctuation models [18]. The 2D image observation of the detection area obtained by the radar can be described as

$$\boldsymbol{z}_k^{(i,j)} = \begin{cases} \sum_{\ell=1}^{\mathcal{M}(k)} \Upsilon\left(\boldsymbol{x}_{k,\ell}\right) \boldsymbol{h}_k^{(i,j)}\left(\boldsymbol{x}_{k,\ell}\right) + v_k^{(i,j)} & \boldsymbol{H}_1\text{: if target is present} \\ v_k^{(i,j)} & \boldsymbol{H}_0\text{: if there is no target} \end{cases} \tag{2}$$

where $\Upsilon\left(\boldsymbol{x}_{k,\ell}\right)$ is the drone' complex amplitude, $\boldsymbol{h}_k^{(i,j)}\left(\boldsymbol{x}_{k,\ell}\right)$ is the nonlinear measurement function which described the intensity' contribution to the cell (i,j), $v_k^{(i,j)} \sim \mathcal{N}(0, \boldsymbol{R}_k)$ is a normal distribution of noise process, and $\boldsymbol{R}_k$ is the measurement covariance matrix. Then, the spread of drone in the data can be described as:

$$\boldsymbol{h}_k^{(i,j)}\left(\boldsymbol{x}_{k,\ell}\right) = \frac{\Delta_x \Delta_y}{2\pi\sigma_h^2} \exp\left[-\frac{\left(i\Delta_x - x_{k,\ell}\right)^2 + \left(j\Delta_y - y_{k,\ell}\right)^2}{2\sigma_h^2}\right] \tag{3}$$

where σ_h is the blurring factor with cell side lengths of Δ_x and Δ_y, then the multi-drone measurement set $\boldsymbol{Z}_k$ can be described as $\boldsymbol{Z}_k = \left\{\boldsymbol{z}_k^{(i,j)} : i = 1 \cdots n_x, j = 1 \cdots n_y\right\}$. Let us consider the noise of measurement is independent. Therefore, the function of likelihood can be described as

$$p\left(\boldsymbol{z}_k^{(i,j)} \middle| \boldsymbol{x}\right) = \begin{cases} \varphi_{(i,j)}\left(\boldsymbol{z}_k^{(i,j)} \middle| \boldsymbol{H}_1\right) \\ \phi_{(i,j)}\left(\boldsymbol{z}_k^{(i,j)} \middle| \boldsymbol{H}_0\right) \end{cases} \tag{4}$$

Let us consider at time k, the drones' fluctuation model are derived to $p\left(\boldsymbol{z}_k^{(i,j)} \middle| \boldsymbol{x}\right)$ and under the consideration of Gaussian process noise, the probability density functions can be described as

$$\begin{aligned} \varphi_{(i,j)}\left(\boldsymbol{z}_k^{(i,j)} \middle| \boldsymbol{H}_1\right) &= \mathcal{N}\left(\boldsymbol{z}_k^{(i,j)}; \sum_{\ell=1}^{\mathcal{M}(k)} \Upsilon\left(\boldsymbol{x}_{k,\ell}\right) \boldsymbol{h}_k^{(i,j)}\left(\boldsymbol{x}_{k,\ell}\right), \boldsymbol{R}\right), \\ \phi_{(i,j)}\left(\boldsymbol{z}_k^{(i,j)} \middle| \boldsymbol{H}_0\right) &= \mathcal{N}\left(\boldsymbol{z}_k^{(i,j)}; 0, \boldsymbol{R}\right) \end{aligned} \tag{5}$$

Assuming the cell' intensity is either Rician distributed if there is a drone target presenting in noise, or Rayleigh distributed if there is only noise present [15,17]. Therefore, for a given $\Upsilon\left(\boldsymbol{x}_{k,\ell}\right) \approx \Upsilon_k$ in the cell (i,j), the probability density functions (PDFs) can be rewritten as

$$\varphi_{(i,j)}\left(\boldsymbol{z}_k^{(i,j)} | \boldsymbol{x}, \boldsymbol{R}, \Upsilon_k\right) = \frac{2\boldsymbol{z}_k^{(i,j)}}{\sigma_{\boldsymbol{R}}^2} exp\left(-\frac{\left[\boldsymbol{z}_k^{(i,j)}\right]^2 + \Upsilon_k^2\left[\boldsymbol{h}_k^{(i,j)}\left(\boldsymbol{x}_{k,\ell}\right)\right]^2}{\sigma_{\boldsymbol{R}}^2}\right) \times I_0\left(\frac{2\boldsymbol{z}_k^{(i,j)}\Upsilon_k \boldsymbol{h}_k^{(i,j)}\left(\boldsymbol{x}_{k,\ell}\right)}{\sigma_{\boldsymbol{R}}^2}\right) \tag{6}$$

$$\phi_{(i,j)}\left(\boldsymbol{z}_k^{(i,j)} | \boldsymbol{R}\right) = \frac{2\boldsymbol{z}_k^{(i,j)}}{\sigma_{\boldsymbol{R}}^2} exp\left(-\frac{\left[\boldsymbol{z}_k^{(i,j)}\right]^2}{\sigma_{\boldsymbol{R}}^2}\right) \tag{7}$$

where $\left(I_0(x) := \sum_{j=0}^{\infty} \frac{\left(x^2/4\right)^j}{j!\Gamma(j+1)}\right)$ is the Bessel function, and $\sigma_{\boldsymbol{R}}^2 = \boldsymbol{R}_k$ is measurement variance. Assuming the detection area is splitted into D cells (resolution) which described by $\boldsymbol{V}_1, \boldsymbol{V}_2, \ldots, \boldsymbol{V}_D \subset \mathbb{R}^{n/2}$, a drone with state $\boldsymbol{x}$ contains a set of cells described by $U(\boldsymbol{x})$. In this paper, we assumed that the drones with a rigid body. That is mean the detection area does not overlap, that is mean, $U(\boldsymbol{x}) \cap U\left(\boldsymbol{x}'\right) = \varnothing$ if $\boldsymbol{x} \neq \boldsymbol{x}'$. Let us consider the measurement values in several cells are conditionally independent of the multi-target state $\boldsymbol{X}_k$. The pdf of $\boldsymbol{Z}_k$ conditioned on $\boldsymbol{X}_k$ by the likelihoods $(\varphi_{(i,j)}, \phi_{(i,j)})$ which are given in (6) and (7) is obtained by:

$$\begin{aligned} g\left(\boldsymbol{Z}_k | \boldsymbol{X}_k, \boldsymbol{R}_k, \Upsilon_k\right) &= \left(\prod_{\boldsymbol{x} \in \boldsymbol{X}_k} \prod_{i,j \in U(\boldsymbol{x})} \varphi_{(i,j)}\left(\boldsymbol{z}_k^{(i,j)} | \boldsymbol{x}, \boldsymbol{R}, \Upsilon\right)\right) \\ &\quad \times \left(\prod_{i,j \notin \cup_{\boldsymbol{x} \in \boldsymbol{X}_k} U(\boldsymbol{x})} \phi_{(i,j)}\left(\boldsymbol{z}_k^{(i,j)} | \boldsymbol{R}\right)\right) \\ &= f\left(\boldsymbol{Z}_k, \boldsymbol{R}\right) \prod_{\boldsymbol{x} \in \boldsymbol{X}_k} g_z(\boldsymbol{x}, \boldsymbol{R}, \Upsilon) \end{aligned} \tag{8}$$

where

$$\begin{aligned} g_z\left(\boldsymbol{x}, \boldsymbol{R}, \Upsilon\right) &= \prod_{i,j \in U(\boldsymbol{x})} \frac{\varphi_{(i,j)}\left(\boldsymbol{z}_k^{(i,j)} | \boldsymbol{x}, \boldsymbol{R}, \Upsilon\right)}{\phi_{(i,j)}\left(\boldsymbol{z}_k^{(i,j)} | \boldsymbol{R}\right)}, \\ f\left(\boldsymbol{Z}_k, \boldsymbol{R}\right) &= \prod_{i,j=1}^{D} \phi_{(i,j)}\left(\boldsymbol{z}_k^{(i,j)} | \boldsymbol{R}\right) \end{aligned} \tag{9}$$

Practically, the drone' detection parameters are mutually time-varying and unknown. For this reason, the drone' pdf cannot be approximated well by the traditional analytical expressions [17]. Therefore, in [7–10] the authors proposed a non-parametric approximation model to reconstruct the pdf of real RCS. This approximation model applied by Legendre orthogonal polynomials (LOP). The first n central moments of real back-scattering are combined by LOPs. Let us consider this model in this work to get an accurate tracking and detection of drone. Let us consider that the drone' back-scattering is random variable $\sigma = \Upsilon_k$ with mean $\overline{\sigma} = \overline{\Upsilon}$, we will use LOP which given in Appendix A. By using this non-parametric approximation model, the new likelihood ratio can be rewritten in terms of Υ_k as

$$g_z\left(\boldsymbol{x}, \boldsymbol{R}, \overline{\Upsilon}\right) = \int g_z\left(\boldsymbol{x}, \boldsymbol{R}, \Upsilon\right) p(\Upsilon_k|\overline{\Upsilon}) d\Upsilon_k \tag{10}$$

Related to the form of (8) and (10), we need a numerical integration scheme. In this work, a MC integration is used to obtain the likelihood ratio as

$$g_z\left(\boldsymbol{x}, \boldsymbol{R}, \overline{\Upsilon}\right) \approx \frac{1}{M}\sum_{m=1}^{M} g_z\left(\boldsymbol{x}, \boldsymbol{R}, \Upsilon_k^m\right) \tag{11}$$

where M is the number of samples and Υ_k^m is known by a random sample from $p(\Upsilon_k|\overline{\Upsilon})$. The prior state of drone ($\boldsymbol{x}$) and w_k are given. While the detection parameters such as $\boldsymbol{R}_k$ and detection probability $p_{D,k}(\boldsymbol{x})$ are considered to be unknown. Also, the w_k, $\boldsymbol{R}_k$ are assumed to be independent. The contribution of this work is to present a new tracking and detection technique for the nonlinear tracking system with hybrid unknown $p_{D,k}(\boldsymbol{x})$ and $\boldsymbol{R}_k$. The approximation of variational Bayesian and Cubature Kalman methods has been proposed here with TBD approach. That is mean to calculate the hybrid posterior distribution of the nonlinear states and $\boldsymbol{R}_k$ by dividing the constant distributions and reconstructing the expressions of the proposed recursive filter.

3. Robust Cubature Kalman multi-Bernoulli-TBD filter

Estimating the variances of measurement ($\boldsymbol{R}_k$) with unknown profile of detection are difficult problems in practice. In addition, the capability of multi-target filters to adaptive learn this nonlinear parameter is very important. A robust Cubature Kalman-Multi-Bernoulli filter for micro-drones tracking is proposed to overcome the limitation caused by high noise effect that traditional methods failed to cope with. The proposed algorithm is more efficiency robust in this case since it is able to work with non-linear tracking systems and unknown $\boldsymbol{R}_k$. Robust adaptive variational approximation algorithm is provided here that is reasonably accurate and efficient. Compared to the standard multi-Bernoulli filter, the proposed algorithm does not assume fixed variances of measurement. This filter generally assumes a more precise specification of the distribution for cardinality of the variances of measurement. Consequently, it is comparatively more tolerant to high noise effect. The proposed algorithm is comparatively more sensitive to low probability of detection, since it does not have prior knowledge of the detection profile with TBD solution. The contribution of this modified technique is to hybrid unknown parameters of detection into one state of drone. By estimate the modified hybrid state of drones, we will get a complete information of drone model, such as a number of drones and kinematic states hybrid with estimated $\boldsymbol{R}$. In the following, we proposed the Variational Bayesian-Cubature Kalman-multi-Bernoulli-TBD recursion for hybrid state.

3.1. The Cubature Kalman approximation

Suppose each drone follows a nonlinear motion and measurement model. The key idea of the Cubature Kalman filtering algorithm is that it uses the third-degree spherical-radial rule to calculate a Gaussian weighted integral. This idea can be described as follows [21]:

$$\int_{\mathbb{R}^j} \Phi(x)\, N(x; 0, \mathrm{I})\, dx \approx \sum_{\ell=1}^{2_j} \omega(\ell)\, \Phi(\xi(\ell)) \tag{12}$$

where $\Phi(x)$ is the known nonlinear function, $\mathrm{I} \in \mathbb{N}_{j\times j}$ is the identity matrix, j is the dimension of the state x, $\xi(\ell)$ is the ℓth cubature point, $\omega(\ell)$ is the weight of the ℓth cubature point, $\omega(\ell) = \frac{1}{2j}$, and $\xi(\ell)$ is the ℓth column of Ψ.

$$\Psi = \sqrt{j}\left\{\underbrace{\begin{pmatrix}1\\ \vdots\\ 0\end{pmatrix}, \ldots \begin{pmatrix}0\\ \vdots\\ 1\end{pmatrix}}_{j}, \underbrace{\begin{pmatrix}-1\\ \vdots\\ 0\end{pmatrix}, \ldots \begin{pmatrix}0\\ \vdots\\ -1\end{pmatrix}}_{j}\right\} \tag{13}$$

3.2. Hybrid state space in TBD fusion

In this section, a closed form solution to the proposed robust Cubature Kalman-Multi-Bernoulli-TBD recursions with unknown profile of detection can be calculated via Cubature Kalman Gaussian mixtures in a similar manner to the conventional Multi-Bernoulli recursion. The nonlinear implementation for the robust Cubature Kalman-Multi-Bernoulli-TBD recursion with unknown noise variance is derived with the products of Cubature Kalman Gaussian mixtures and Inverse-Gamma. The kinematic state part ($\boldsymbol{x}$) and the hybrid part of the noise variance ($\boldsymbol{R}$) are modelled by Cubature Kalman Gaussian distribution and the Inverse-Gamma distribution, respectively. The decomposition of the Multi-Bernoulli-TBD posterior distribution into the separate Inverse-Gamma and Cubature Kalman Gaussian components allows the concept of variational approximation algorithm. Define the novel hybrid state space of a drone target as:

$\boldsymbol{\Phi}_{\boldsymbol{x},k|k-1}(\boldsymbol{x}|\mathbb{x})$ = The drone transition density for kinematic state, given previous state value $\mathbb{x}$

$\boldsymbol{\Phi}_{\boldsymbol{R},k|k-1}\left(\boldsymbol{R}|\grave{\boldsymbol{R}}\right)$ = The drone transition density for noise variance, given previous $\grave{\boldsymbol{R}}$

$\boldsymbol{\Phi}_{k|k-1}\left(\boldsymbol{x}, \boldsymbol{R}|\mathbb{x}, \grave{\boldsymbol{R}}\right) = \boldsymbol{\Phi}_{\boldsymbol{R},k|k-1}\left(\boldsymbol{R}|\grave{\boldsymbol{R}}\right)\boldsymbol{\Phi}_{\boldsymbol{x},k|k-1}(\boldsymbol{x}|\mathbb{x})$ = The drone transition density for novel hybrid state, based on $\grave{\boldsymbol{R}}$, $\mathbb{x}$ values at time $k-1$

3.3. Robust Cubature Kalman multi-Bernoulli-TBD recursions

Robust Cubature Kalman multi-Bernoulli-TBD prediction: Let us considering the hybrid posterior distribution at time $k-1$ is described as a multi-Bernoulli form [1–3] with the existence probability $r^{(i)} \in (1, 0)$ and probability of density $p^{(i)}, i = 1, \ldots, M$, where M is the multi-Bernoulli random finite set, i.e., $\pi = \left\{r^{(i)}, P^{(i)}(\boldsymbol{x}, \boldsymbol{R})\right\}_{i=1}^{M}$. Let us consider that $\boldsymbol{R}$ and $\boldsymbol{x}$ are assumed to be independent, and the probability of survival $p_{s,k}(\boldsymbol{x}, \boldsymbol{R})$ is also independent, thus $p_{s,k}(\boldsymbol{x}, \boldsymbol{R}) = p_{s,k}$, we can get the hybrid posterior distribution at time $k-1$ by the parameters of Cubature Kalman multi-Bernoulli-TBD as

$$\pi_{k-1} = \left\{\left(r_{k-1}^{(i)}, p_{k-1}^{(i)}\left(\mathbb{x}, \grave{\boldsymbol{R}}\right)\right)\right\}_{i=1}^{M_{k-1}} \tag{14}$$

where M_{k-1} known by the tracks' number at $k-1$, then the predicted distribution is Cubature Kalman multi-Bernoulli-TBD obtained by the predicted and birth components

$$\pi_{k|k-1} = \left\{\left(r^{(i)}_{P,k|k-1}, p^{(i)}_{P,k|k-1}\right)\right\}_{i=1}^{M_{k-1}} \cup \left\{\left(r^{(i)}_{\Gamma,k}, p^{(i)}_{\Gamma,k}\right)\right\}_{i=1}^{M_{\Gamma,k}} \tag{15}$$

where $\left\{\left(r^{(i)}_{P,k|k-1}, p^{(i)}_{P,k|k-1}\right)\right\}_{i=1}^{M_{k-1}}$ and $\left\{\left(r^{(i)}_{\Gamma,k}, p^{(i)}_{\Gamma,k}\right)\right\}_{i=1}^{M_{\Gamma,k}}$ describe the RFS parameters of Cubature Kalman multi-Bernoulli-TBD for the predicted drones and births, respectively. $M_{\Gamma,k}$ known by predicted number of births track of, then

$$r^{(i)}_{P,k|k-1} = r^{(i)}_{k-1}\left\langle p^{(i)}_{k-1}, p_{s,k}\right\rangle \tag{16}$$

$$p^{(i)}_{P,k|k-1}(\boldsymbol{x},\boldsymbol{R}) = \frac{\left\langle \Phi_{k|k-1}(\boldsymbol{x},\boldsymbol{R}|\cdot), p^{(i)}_{k-1}p_{s,k}\right\rangle}{\left\langle p^{(i)}_{k-1}, p_{s,k}\right\rangle} \tag{17}$$

where $\langle\cdot,\cdot\rangle$ describe the operation of inner product. The overall number of tracks for prediction is $M_{k|k-1} = M_{k-1} + M_{\Gamma,k}$.

Robust Cubature Kalman multi-Bernoulli-TBD update: Let us consider that the hybrid prediction distribution of targets at time k is a Cubature Kalman multi-Bernoulli-TBD in $\pi_{k|k-1} = \left\{\left(r^{(i)}_{k|k-1}, p^{(i)}_{k|k-1}\right)\right\}_{i=1}^{M_{k|k-1}}$ and given the image observation' measurements at time k, $(\boldsymbol{Z}_k)$. Then, the updated Multi-Bernoulli-TBD parameters are given by

$$\pi_k \cong \left\{\left\{r^{(i)}_k(\boldsymbol{z}), p^{(i)}_k(\boldsymbol{x},\boldsymbol{R};\boldsymbol{z})\right\}_{z\in\boldsymbol{Z}_k}\right\}_{i=1}^{M_{k/k-1}} \tag{18}$$

where

$$\begin{aligned} r^{(i)}_k(\boldsymbol{z}) &= \frac{r^{(i)}_{k|k-1}\left\langle p^{(i)}_{k|k-1}(\boldsymbol{x},\boldsymbol{R}), g_z(\boldsymbol{x},\boldsymbol{R})\right\rangle}{1 - r^{(i)}_{k|k-1} + r^{(i)}_{k|k-1}\left\langle p^{(i)}_{k|k-1}(\boldsymbol{x},\boldsymbol{R}), g_z(\boldsymbol{x},\boldsymbol{R})\right\rangle}, \\ p^{(i)}_k(\boldsymbol{x},\boldsymbol{R};\boldsymbol{z}) &= \frac{p^{(i)}_{D,k}(\boldsymbol{x},\boldsymbol{R}|\boldsymbol{z})}{\left\langle p^{(i)}_{k|k-1}, g_z(\boldsymbol{x},\boldsymbol{R})\right\rangle} \end{aligned} \tag{19}$$

where $p^{(i)}_{D,k}(\boldsymbol{x},\boldsymbol{R}|\boldsymbol{Z}_k)$ denoted by the hybrid posterior distribution and $p^{(i)}_{D,k}(\boldsymbol{x},\boldsymbol{R}|\boldsymbol{Z}_k) = p^{(i)}_{k|k-1}(\boldsymbol{x},\boldsymbol{R})\cdot g_z(\boldsymbol{x},\boldsymbol{R})$. Let us consider $\boldsymbol{R}$ and $\Phi_{\boldsymbol{R},k|k-1}\left(\boldsymbol{R}|\grave{\boldsymbol{R}}\right)$ are assumed to be unknown and the $\boldsymbol{Z}_k$ is known. Although, $p^{(i)}_{D,k}(\boldsymbol{x},\boldsymbol{R}|\boldsymbol{Z}_k)$ is intractable analytically, then we cannot get the analytical expression. To make the coupled update step tractable, the VB method [16–20] has been presented to obtaining the posterior $p^{(i)}_{D,k}(\boldsymbol{x},\boldsymbol{R}|\boldsymbol{Z}_k)$. Let us consider that $p^{(i)}_{D,k}(\boldsymbol{x},\boldsymbol{R}|\boldsymbol{Z}_k)$ can be described by two approximate posteriors $\boldsymbol{q}_{\boldsymbol{x},k}(\boldsymbol{x})$ and $\boldsymbol{q}_{\boldsymbol{R},k}(\boldsymbol{R})$ for $\boldsymbol{x}$ and $\boldsymbol{R}$ respectively. Thus, $p^{(i)}_{D,k}(\boldsymbol{x},\boldsymbol{R}|z) = \boldsymbol{q}_{\boldsymbol{x},k}(\boldsymbol{x})\,\boldsymbol{q}_{\boldsymbol{R},k}(\boldsymbol{R})$. To obtain an accurate approximation of $p^{(i)}_{D,k}(\boldsymbol{x},\boldsymbol{R}|z)$, the divergence of Kullback–Leibler (KL) is presented as [16–20]:

$$\begin{aligned} \hat{\boldsymbol{q}}_{\boldsymbol{x},k}(\boldsymbol{x}), \hat{\boldsymbol{q}}_{\boldsymbol{R},k}(\boldsymbol{R}) &= \underset{\boldsymbol{q}_{\boldsymbol{x},k}\boldsymbol{q}_{\boldsymbol{R},k}}{\arg\ \min}(\mathfrak{R}), \\ \mathfrak{R} &= KL\left[\boldsymbol{q}_{\boldsymbol{x},k}(\boldsymbol{x})\,\boldsymbol{q}_{\boldsymbol{R},k}(\boldsymbol{R}) \parallel p^{(i)}_{D,k}(\boldsymbol{x},\boldsymbol{R}|z)\right] \end{aligned} \tag{20}$$

where

$$\begin{aligned} &KL\left[\boldsymbol{q}_{\boldsymbol{x},k}(\boldsymbol{x})\,\boldsymbol{q}_{\boldsymbol{R},k}(\boldsymbol{R}) \parallel p^{(i)}_{D,k}(\boldsymbol{x},\boldsymbol{R}|z)\right] \\ &= \int \boldsymbol{q}_{\boldsymbol{x},k}(\boldsymbol{x})\,\boldsymbol{q}_{\boldsymbol{R},k}(\boldsymbol{R}) \log\left(\frac{\boldsymbol{q}_{\boldsymbol{x},k}(\boldsymbol{x})\,\boldsymbol{q}_{\boldsymbol{R},k}(\boldsymbol{R})}{p^{(i)}_{D,k}(\boldsymbol{x},\boldsymbol{R}|z)}\right) d\boldsymbol{x}d\boldsymbol{R} \end{aligned} \tag{21}$$

The analytical expression for $\hat{\boldsymbol{q}}_{\boldsymbol{x},k}(\boldsymbol{x})$ and $\hat{\boldsymbol{q}}_{\boldsymbol{R},k}(\boldsymbol{R})$ are obtained as [20]:

$$\log\hat{\boldsymbol{q}}_{\boldsymbol{x},k}(\boldsymbol{x}) = E_{\hat{\boldsymbol{q}}_{\boldsymbol{R},k}}\left[\log p_{D,k}(\boldsymbol{x},\boldsymbol{R}|z_{1:k-1})\right] + c_{\boldsymbol{x}},$$

$$\log\hat{\boldsymbol{q}}_{\boldsymbol{R},k}(\boldsymbol{R}) = E_{\hat{\boldsymbol{q}}_{\boldsymbol{x},k}}\left[\log p_{D,k}(\boldsymbol{x},\boldsymbol{R}|z_{1:k-1})\right] + c_{\boldsymbol{R}} \tag{22}$$

where $c_{\boldsymbol{R}}$ and $c_{\boldsymbol{x}}$ are the fixed values related to $\boldsymbol{R}$ and x. The predicted values on (22) are calculated by the previous estimated values of $\boldsymbol{q}_{\boldsymbol{x},k}(\boldsymbol{x})$ and $\boldsymbol{q}_{\boldsymbol{R},k}(\boldsymbol{R})$ to get the next variables [20]. Due to the joint of $\boldsymbol{q}_{\boldsymbol{x},k}(\boldsymbol{x})$ and $\boldsymbol{q}_{\boldsymbol{R},k}(\boldsymbol{R})$, therefore they also cannot be calculated directly. Let us considering the same as the calculation of variational in [19,20], we can get the derivations where $\boldsymbol{q}_{\boldsymbol{R},k}(\boldsymbol{R})$ and $\boldsymbol{q}_{\boldsymbol{x},k}(\boldsymbol{x})$ are the forms of integral in inverse Gamma and Gaussian distributions, as:

$$\begin{aligned} \boldsymbol{q}_{\boldsymbol{x},k}(\boldsymbol{x}) &= \int N\left(\mathbb{x};\boldsymbol{m}_k = \hat{\boldsymbol{x}}_k, \boldsymbol{P}_k\right) d\mathbb{x}, \qquad \boldsymbol{q}_{\boldsymbol{R},k}(\boldsymbol{R}) \\ &= \int\left(\prod_{l=1}^{d}\text{Inv}-\text{Gamma}(\sigma^2_{k,l};\alpha_{k,l},\beta_{k,l})\right) d\sigma_{k,l} \end{aligned} \tag{23}$$

where 'd' describes the size of $\boldsymbol{R}_k$. $\text{Inv}-\text{Gamma}(\cdot;\alpha,\beta)$ describes the Inverse-Gamma distribution of, $\boldsymbol{R}_k$, where the degree of freedom is α_k and the scaling parameter is β_k, thus

$$\text{Inv}-\text{Gamma}(\boldsymbol{R};\alpha,\beta) = \frac{\beta^{\alpha}}{\Gamma(\alpha)}\boldsymbol{R}^{-\alpha-1}\exp\left(-\frac{\beta}{\boldsymbol{R}}\right) \tag{24}$$

where

$$\Gamma(\alpha) = \int_0^{\infty} t^{\alpha-1}\exp(-t)\,dt$$

and $\hat{\boldsymbol{R}}_k = diag\left(\beta_{k,1}/\alpha_{k,1}, \ldots, \beta_{k,d}/\alpha_{k,d}\right)$.

4. CK-GIGM-TBD implementation of VB-Cubature Kalman-multi-Bernoulli-TBD filter

The jth Gaussian mixtures component can be achieved by computing its mean $m^{(i,j)}_k$, covariance $P^{(i,j)}_k$ and the Inverse-Gamma mixture' parameters $(\alpha^{(i,j)}_{k,l}, \beta^{(i,j)}_{k,l})$. When each parameter of $m^{(i,j)}_k$, $P^{(i,j)}_k$, $\alpha^{(i,j)}_{k,l}$, $\beta^{(i,j)}_{k,l}$ are achieved, the multi-Bernoulli posterior density of the ith target can be calculated. However, in traditional Gaussian Inverse-Gamma mixture-MB (GIGM-MB) approach, these components are computed under the linear model. For extending GIGM-MB approach into nonlinear scenarios, we utilize the CK method into our approach for its significant tracking performance in the nonlinear cases. We use the CK method to predict states and covariance. The CK method of uses observations (each observation denotes one possible target) to update predicted observation. We use the ith cell to denote observations generated by the same drone. For updating the predicted observation of the drones by the CK method, the ith cell set should be converted into the observation set. Therefore, the CK method can be used to approximate the states and covariances of the drones. Using the approximated states and covariances, the CK-GIGM-MB mixtures of the VB-CK-MB-TBD approach can be achieved for estimating states of drones. From the above operations, the tracking performance of the traditional GIGM-MB approach in nonlinear TBD scenarios can be significantly improved. Observed that both of the probability densities $p^{(i)}_{k|k-1}(\boldsymbol{x},\boldsymbol{R})$ and $p^{(i)}_k(\boldsymbol{x},\boldsymbol{R};\boldsymbol{z})$ consist of CK-GIGM-MB components; these components can be given by computing their means, covariances and Inverse-Gamma parameters. This implementation consists of prediction and update steps. In the next, the Robust Cubature Kalman multi-Bernoulli-TBD implementation based on CK-GIGM-MB is discussed. With the decomposition of the distribution of multi-Bernoulli-TBD separated into Cubature Kalman Gaussian and Inverse-Gamma components, the closed-form solutions to the proposed robust Cubature Kalman multi-Bernoulli-TBD filter are derived by using the VB approximations. The solving problem

is based on a CK-GIGM-MB approximation of the multi-Bernoulli RFS representation of a drones' pdf. That is,

$$\pi_k(\boldsymbol{X}) \sim \left\{\left(r_k^{(i)}, p_k^{(i)}(\boldsymbol{x},\boldsymbol{R})\right)\right\}_{i=1}^{M_k} = \left\{r_k^{(i)}, \left\{w_k^{(i,j)}, m_k^{(i,j)}, P_k^{(i,j)}, \alpha_{k,l}^{(i,j)}, \beta_{k,l}^{(i,j)}\right\}_{j=1}^{J_k^{(i)}}\right\}_{i=1}^{M_k} \quad (25)$$

where $\boldsymbol{J}_k^{(i)}$ known by CK-GIGM-MB mixers' number of the ith target, $w_k^{(i,j)}$ known by the jth component' weight, $\left(\alpha_{k,l}^{(i,j)}, \beta_{k,l}^{(i,j)}\right)$ known by the parameters of Inv-Gamma distribution to estimate $\boldsymbol{R}_k$, and $\left(m_k^{(i,j)}, P_k^{(i,j)}\right)$ known by the components of Gaussian distribution (mean, covariance). Here, each Bernoulli-TBD RFS pdf $p_{k-1}^{(i)}(\boldsymbol{x},\boldsymbol{R})$ at time $k-1$ is approximated by a CK-GIGM $\left\{w_k^{(i,j)}, m_k^{(i,j)}, P_k^{(i,j)}, \alpha_{k,l}^{(i,j)}, \beta_{k,l}^{(i,j)}\right\}_{j=1}^{J_k^{(i)}}$ as:

$$p_{k-1}^{(i)}(\boldsymbol{x},\boldsymbol{R}) = \sum_{j=1}^{J_{k-1}^{(i)}} w_{k-1}^{(i,j)} N\left(\boldsymbol{x}; m_{k-1}^{(i,j)}, P_{k-1}^{(i,j)}\right) \times \prod_{l=1}^{d^{(i,j)}} \text{Inv}-\text{Gamma}\left(\left(\sigma_{k-1,l}^{(i,j)}\right)^2; \alpha_{k-1,l}^{(i,j)}, \beta_{k-1,l}^{(i,j)}\right) \quad (26)$$

where $\alpha_{k-1,l}^{(i,j)}$ and $\beta_{k-1,l}^{(i,j)}$ are the parameters of Inv-Gamma distribution to the estimate $\boldsymbol{R}_{k-1}$, and $\boldsymbol{R}_{k-1}^{(i,\jmath)} = diag\left[\frac{\beta_{k-1,1}^{(i,\jmath)}}{\alpha_{k-1,1}^{(i,\jmath)}}, \ldots, \frac{\beta_{k-1,d}^{(i,\jmath)}}{\alpha_{k-1,d}^{(i,\jmath)}}\right]$. In addition, assuming the proposed CK-GIGM-MB-TBD posterior at time $k-1$ is described as follows:

$$\pi_{k-1}(\boldsymbol{X},\boldsymbol{R}) \sim \left\{\left(r_{k-1}^{(i)}, p_{k-1}^{(i)}(\boldsymbol{x},\boldsymbol{R})\right)\right\}_{i=1}^{M_{k-1}} = \left\{r_{k-1}^{(i)}, \left\{\boldsymbol{x}_{k-1}^{(i,j)}, w_{k-1}^{(i,j)}, \left\{\alpha_{k-1,l}^{(i,j)}, \beta_{k-1,l}^{(i,j)}\right\}_{l=1}^{d}\right\}_{j=1}^{J_{k-1}^{(i)}}\right\}_{i=1}^{M_{k-1}} \quad (27)$$

4.1. CK-GIGM-MB-TBD prediction

The set of new birth Bernoulli-RFS $\left\{r_{\Gamma,k}^{(i)}, p_{\Gamma,k}^{(i)}(\boldsymbol{x},\boldsymbol{R})\right\}_{i=1}^{M_{\Gamma,k}}$ where $p_{\Gamma,k}^{(i)}, i = 1,\ldots,M_{\Gamma,k}$ is formed using CK-GIGM-MB-TBD approximations to the birth set pdfs given by:

$$p_{\Gamma,k}^{(i)}(\boldsymbol{x},\boldsymbol{R}) = \sum_{j=1}^{J_{\Gamma,k}^{(i)}} w_{\Gamma,k}^{(i,j)} N\left(\boldsymbol{x}; m_{\Gamma,k}^{(i,j)}, P_{\Gamma,k}^{(i,j)}\right) \times \prod_{l=1}^{d^{(i,j)}} \text{Inv}-\text{Gamma}\left(\left(\sigma_{\Gamma,k,l}^{(i,j)}\right)^2; \alpha_{\Gamma,k,l}^{(i,j)}, \beta_{\Gamma,k,l}^{(i,j)}\right) \quad (28)$$

where $w_{\Gamma,k}^{(i,j)}, \alpha_{\Gamma,k,l}^{(i,j)}, \beta_{\Gamma,k,l}^{(i,j)}$ known by the birth model parameters according to the ith target. Let us consider that the probability of survival targets is independent of state, i.e. $p_{S,k}(\boldsymbol{x}) = p_{S,k}$. Thus, the predicted CK-GIGM-MB-TBD posterior distribution $\pi_{k|k-1}(\boldsymbol{X},\boldsymbol{R}) = \left\{\left(r_{P,k|k-1}^{(i)}, p_{P,k|k-1}^{(i)}(\boldsymbol{x},\boldsymbol{R})\right)\right\}_{i=1}^{M_{k-1}} \cup \left\{\left(r_{\Gamma,k}^{(i)}, p_{\Gamma,k}^{(i)}(\boldsymbol{x},\boldsymbol{R})\right)\right\}_{i=1}^{M_{\Gamma,k}}$ is given by

$$r_{P,k|k-1}^{(i)} = r_{k-1}^{(i)} p_{S,k} \quad (29)$$

$$p_{P,k|k-1}^{(i)}(\boldsymbol{x},\boldsymbol{R}) = \sum_{j=1}^{J_{k-1}^{(i)}} w_{k-1}^{(i,j)} N\left(\boldsymbol{x}; m_{P,k|k-1}^{(i,j)}, P_{P,k|k-1}^{(i,j)}\right) \times \prod_{l=1}^{d^{(i,j)}} \text{Inv}-\text{Gamma}\left(\left(\sigma_{P,k|k-1,l}^{(i,j)}\right)^2; \alpha_{P,k|k-1,l}^{(i,j)}, \beta_{P,k|k-1,l}^{(i,j)}\right) \quad (30)$$

Here, we will use $m_{k-1}^{(i,j)}$ and $P_{k-1}^{(i,j)}$ to predict $m_{P,k|k-1}^{(i,j)}$ and $P_{P,k|k-1}^{(i,j)}$. These values are calculated by a group of cubature points. With the achieved $m_{P,k|k-1}^{(i,j)}$ and $P_{P,k|k-1}^{(i,j)}$, the predicted probability density $p_{P,k|k-1}^{(i)}(\boldsymbol{x},\boldsymbol{R})$ in (30) could be calculated. According to the cubature rule [21], the $\jmath$ -dimensional Gaussian weighted integral can be given by

$$\int_{\mathbb{R}^\jmath} \Phi(x) N(x; m, \mathrm{P})\, dx \approx \frac{1}{2\jmath} \sum_{\ell=1}^{2\jmath} \Phi\left(m + \sqrt{\mathrm{P}}\Psi_\jmath\right), \quad (31)$$

where $\Psi_\jmath$ is computed by (13), using the above cubature rule, the ℓth cubature point at time step $k-1$ can be defined by

$$\chi_{k-1}^{(i,j)}(\ell) = m_{k-1}^{(i,j)} + \mathbb{C}_{K-1}^{(i,j)} \xi(\ell) \quad (32)$$

where $\mathbb{C}_{K-1}^{(i,j)} = \textbf{chol}\left[P_{k-1}^{(i,j)}\right]^T$, "**chol**" denotes the Cholesky decomposition,

$$\chi_{k-1}^{(i,j)}(\ell) = m_{k-1}^{(i,j)} + \mathbb{C}_{K-1}^{(i,j)} \xi(\ell) \quad (33)$$

$\ell = 1,\ldots,2\jmath$, $\jmath$ is the dimension of state $m_{k-1}^{(i,j)}$, $\xi(\ell)$ is the ℓth column of Ψ, Ψ can be obtained according to Eq. (13). Then, the cubature set can be represented by $\left\{\chi_{k-1}^{(i,j)}(\ell)\right\}_{\ell=1}^{2\jmath}$ and $\chi_{k|k-1}^{(i,j)}(\ell) = \Phi_{k-1}\left(\chi_{k-1}^{(i,j)}(\ell)\right)$. Using the cubature set, the predicted $m_{P,k/k-1}^{(i,j)}$ and $P_{P,k|k-1}^{(i,j)}$ can be calculated by

$$m_{P,k/k-1}^{(i,j)} = \frac{1}{2\jmath} \sum_{\ell=1}^{2\jmath} \chi_{k|k-1}^{(i,j)}(\ell) \quad (34)$$

$$P_{P,k|k-1}^{(i,j)} = \frac{1}{2\jmath} \sum_{\ell=1}^{2\jmath} \left(m_{P,k|k-1}^{(i,j)} - \chi_{k|k-1}^{(i,j)}(\ell)\right) \times \left(m_{P,k|k-1}^{(i,j)} - \chi_{k|k-1}^{(i,j)}(\ell)\right)^T + \mathbf{Q}_{k-1} \quad (35)$$

Also, we can compute the predicted parameters of Inverse-Gamma distribution as:

$$\alpha_{P,k|k-1,l}^{(i,j)} = \rho_l^{(i,j)} \alpha_{k-1,l}^{(i,j)}, \qquad \beta_{P,k|k-1,l}^{(i,j)} = \rho_l^{(i,j)} \beta_{k-1,l}^{(i,j)} \quad (36)$$

where $\hat{R}_{P,k|k-1}^{(i,j)} = diag\left(\beta_{P,k|k-1,1}^{(i,j)}/\alpha_{P,k|k-1,1}^{(i,j)}, \ldots, \beta_{P,k|k-1,d}^{(i,j)}/\alpha_{P,k|k-1,d}^{(i,j)}\right)$, $l = 1,\ldots,d$ and $\rho_l^{(i,j)}$ known by the factor to accommodate the time-fluctuations of $\boldsymbol{R}_k$, which effects of the estimation of $\boldsymbol{R}_k$, $\rho_l \in (0,1]$. If ρ_l is high, that is mean a slow fluctuation in time. Furthermore, for small ρ_l, $\boldsymbol{R}_k$ should be with high fluctuations [18–20].

4.2. CK-GIGM-MB-TBD updating

Let us consider that the prediction of CK-GIGM-MB-TBD posterior distribution $\pi_{k|k-1}(\boldsymbol{X},\boldsymbol{R}) = \left\{\left(r_{k|k-1}^{(i)}, p_{k|k-1}^{(i)}(\boldsymbol{x},\boldsymbol{R})\right)\right\}_{i=1}^{M_{k|k-1}}$ is obtained at time k, where $p_{k|k-1}^{(i)}, (i = 1,\ldots,M_{k|k-1})$ is obtained by CK-Gaussian and inverse Gamma mixtures as

$$p_{k|k-1}^{(i)}(\boldsymbol{x},\boldsymbol{R}) = \sum_{j=1}^{J_{k|k-1}^{(i)}} w_{k|k-1}^{(i,j)} N\left(\boldsymbol{x}; m_{k|k-1}^{(i,j)}, P_{k|k-1}^{(i,j)}\right) \times \prod_{l=1}^{d^{(i,j)}} \text{Inv}-\text{Gamma}\left(\left(\sigma_{k|k-1,l}^{(i,j)}\right)^2; \alpha_{k|k-1,l}^{(i,j)}, \beta_{k|k-1,l}^{(i,j)}\right) \quad (37)$$

$$r_k^{(i)}(z) = \frac{r_{k|k-1}^{(i)} e_k^{(i)}(\boldsymbol{R}, z)}{1 - r_{k|k-1}^{(i)} + r_{k|k-1}^{(i)} e_k^{(i)}(\boldsymbol{R}, z)},$$
$$p_k^{(i)}(\boldsymbol{x}, \boldsymbol{R}; \boldsymbol{z}) = \frac{\sum_{j=1}^{J_{k|k-1}^{(i)}} w_{k|k-1}^{(i,j)} N\left(\boldsymbol{x}; m_k^{(i,j)}, P_k^{(i,j)}\right) \prod_{l=1}^{d^{(i,j)}} \text{Inv} - \text{Gamma}\left(\left(\sigma_{k,l}^{(i,j)}\right)^2; \alpha_{k,l}^{(i,j)}, \beta_{k,l}^{(i,j)}\right)}{\sum_{j=1}^{J_{k|k-1}^{(i)}} w_{k|k-1}^{(i,j)}} \quad (38)$$

Box I.

Then, the updating posterior $\pi_k(\boldsymbol{X}, \boldsymbol{R}) = \left\{\left\{r_k^{(i)}(\boldsymbol{z}), p_k^{(i)}(\boldsymbol{x}, \boldsymbol{R}; \boldsymbol{z})\right\}_{\boldsymbol{z} \in \boldsymbol{Z}_k}\right\}_{i=1}^{M_{k/k-1}}$ can be calculated as Eq. (38) given in Box I.

Then, we can obtain the parameters of updating by next iteration. The initiation set for $l = 1, \ldots, d$ are $m_k^{(i,j)(0)} = m_{k|k-1}^{(i,j)}$, $p_k^{(i,j)(0)} = p_{k|k-1}^{(i,j)}$, $\alpha_{k,l}^{(i,j)} = 0.5 + \alpha_{k|k-1,l}^{(i,j)}$, $\beta_{k,l}^{(i,j)(0)} = \beta_{k|k-1,l}^{(i,j)}$. Finally, the iteration is obtained in Appendix B.

4.3. Computational complexity of the proposed CK-GIGM-MB-TBD filter

The multi-Bernoulli (MB)-TBD filter with a sequential Monte Carlo (SMC) implementation has been used to the nonlinear tracking for small target with good performance. But, all of them have an equivalent problem of slow adaptation to variances of the measurement with a heavy computation. This kind of approach brings an amount of computation and causes the overestimation of the target number. In addition to, the filtering accuracy of the SMC-MB-TBD filter is the worst, due to the small particles number for each tracks. Moreover since the SMC-MB-TBD calculation requires a sum involving pairs of particles in the transition density, the implementation has a computational complexity of $\mathcal{O}(N^2)$, where N is the number of particles [3]. For example, in this paper, we use $N = 1000$ birth particles and $N = 1000$ continuing particles to simulate the SMC-MB-TBD algorithm. Furthermore, an outsized number of particles mean an outsized amount of calculation. This may limit the performance real-time of the proposed CK-GIGM-MB-TBD filtering. In this approach, we present an efficient cubature rule for Gaussian weighted integrals. Furthermore, we calculate a third-degree fully symmetric cubature rule which features a linear increasing of complexity in terms of function evaluations with the dimension ($\jmath$). Accurately, a group of cubature points and weights are chosen in order that the cubature rule is adequate to a group of monomials of degree three ($d = 3$) or less. The good performance nonlinear filter could be applied to unravel nonlinear filtering problems with high-dimensional and minimal computational effort is presented. The CK-GIGM-MB-TBD filter solution in the Gaussian domain reduces to the matter of the way to calculate multi-dimensional integrals, whose integrands are all of the expression *Gaussian density* × *nonlinear function*. The complexity of the CK-GIGM-MB-TBD recursion is linear within the number of measurements and targets. Here, we are mentioned that the cubature rule is the choice approach to resolve this effective problem. The cubature rule entails $2\jmath$ cubature points, where $\jmath$ is the dimension of state-vector; here, we are needed to calculate $2\jmath$ functional evaluations at each update cycle. The computational complexity scales is linear with the dimension $\jmath$ in terms of the functional evaluations whereas it grows cubically in terms of flops. The computational complexity is approximately $\mathcal{O}(2\jmath) \ll \mathcal{O}(N^2)$(SMC-MB-TBD). Hence, the CK-GIGM-MB-TBD eases the burden on the curse of dimensionality. However, it is not a complete remedy for the dimensionality issue. During this approach, assuming that we have a cubature rule of degree three ($d = 3$). In this approach, we consider that ($\jmath = 20$ and $d = 3$). Therefore, we can calculate the cubature rule which contains of the cubature points by compute only a pair of moment equations.

5. Pruning and merging of proposed filter

Pruning and merging of mixture components are required to prevent an unbounded growth. From the prediction and correction, one can realize that as time passes, the number of proposed posterior components increases rapidly, it costs the computation very much. To keep the number of components at a tractable level, pruning and merging of the proposed posterior components perform simultaneously [16,26]. Component pruning is performed by removing mixture components whose variances of measurement fall above a predetermined threshold T', as $\left\|\boldsymbol{R}_k^{(i,j)}\right\|_2 < T'$. Component merging is performed by confining Hellinger distance between two proposed posterior components $(\jmath, j)$ as $0 < d_{\jmath j} < 1$ [see (39) as given in Box II]. Empirically we found that the merging threshold must be chosen conservatively to avoid merging proposed posterior components of spatially closed drones, because merging such components may cause cardinality error. This similar measure is used to identify groups of mixture components under a certain threshold $\mathbb{S}'$. Consequently, the entire group indexed by $I = \left\{\jmath : d_{\jmath j} < \mathbb{S}'\right\}$ of reference component (j) is replaced by a one posterior component with matching mean $\left(\tilde{\mu}_{\beta,k}, \tilde{m}_k\right)$ and approximate covariance $\left(\left[\tilde{\sigma}_{\beta,k}\right]^2, \tilde{p}_k\right)$. The details of implemented pruning and merging scheme are given below in Table 1.

6. Simulations and results

In this section, we present the simulations and results of a proposed robust Cubature Kalman-multi-Bernoulli-TBD filter. A non-linear multi-drone tracking scenario is used to performance demonstration of the proposed CK-GIGM-MB-TBD filter versus the multi-Bernoulli-TBD [14] and variational Bayesian-multi-Bernoulli [20] filters.

6.1. Modelling and tracking of drones

A complex drone' RCS is calculated by the combination of the RCSs with simple structures. In [5], the authors presented a real simulation for RCS of a complex targets. According to the variations in target motion, aspect angle, and orientation the measured RCS will be fluctuated during their flight. As shown in Fig. 2, three numbers of drones with size' different such as Inspire 1 (DJI), Hexacopter (DJI S900), and Phantom 3 (DJI). The drone fluctuation model will be used for performance prediction

$$d_{\jmath j} = \sqrt{1 - \left[\frac{\sqrt{N\left(0; \left[m_k^{(i,\jmath)}\left(\boldsymbol{R}_k^{(i,\jmath)}\right) - m_k^{(i,j)}\left(\boldsymbol{R}_k^{(i,j)}\right)\right], \left[P_k^{(i,\jmath)}\left(\boldsymbol{R}_k^{(i,\jmath)}\right) + P_k^{(i,j)}\left(\boldsymbol{R}_k^{(i,j)}\right)\right]\right)}}{\left(\det 8\pi \left(\left[P_k^{(i,\jmath)}\left(\boldsymbol{R}_k^{(i,\jmath)}\right)\right]^{-1} + \left[P_k^{(i,j)}\left(\boldsymbol{R}_k^{(i,j)}\right)\right]^{-1}\right)\right)^{1/4}} \right] \tag{39}$$

Box II.

Table 1
Pseudocode for proposed filter Pruning and Merging for *i*th Drone.

input: A predetermined threshold T′, a merging threshold $\mathbb{S}'$, a maximum allowable number of proposed posterior components $J_{\max}^{(i)}$ and proposed posterior components $\left\{W_k^{(i,j)}, m_k^{(i,j)}, P_k^{(i,j)}, \alpha_k^{(i,j)}, \beta_k^{(i,j)}\right\}_{j=1}^{J_k^{(i)}}$.
initialize: Set $\ell \leftarrow 0$ and $I \leftarrow \left\{\jmath = 1, \ldots, J_k^{(i)} \middle| \left\|\boldsymbol{R}_k^{(i,\jmath)}\right\|_2 < \mathrm{T}'\right\}$, where $\boldsymbol{R}_k^{(i,\jmath)} = diag\left[\frac{\beta_{k,1}^{(i,\jmath)}}{\alpha_{k,1}^{(i,\jmath)}}, \ldots, \frac{\beta_{k,d}^{(i,\jmath)}}{\alpha_{k,d}^{(i,\jmath)}}\right]$.
repeat:
$\ell \leftarrow \ell + 1$
$j \leftarrow \arg\max_{\jmath \in I} W_k^{(i,\jmath)}$
$L \leftarrow \left\{\jmath \in I | d_{\jmath j} < \mathbb{S}'\right\}$, $0 < d_{\jmath j} < 1$
$\tilde{W}_{k|k}^{(i,\ell)} \leftarrow \sum_{\jmath \in L} W_k^{(i,\jmath)}$
$\tilde{m}_k^{(i,\ell)} \leftarrow \frac{1}{\tilde{W}_k^{(i,\ell)}} \sum_{\jmath \in L} W_k^{(i,\jmath)} m_k^{(i,\jmath)}$
$\tilde{P}_k^{(i,\ell)} \leftarrow \frac{1}{\tilde{W}_k^{(i,\ell)}} \sum_{\jmath \in L} W_k^{(i,\jmath)} \cdot \left(P_k^{(i,\jmath)} + \left(\tilde{m}_k^{(i,\ell)} - m_k^{(i,\jmath)}\right)\left(\tilde{m}_k^{(i,\ell)} - m_k^{(i,\jmath)}\right)^T\right)$
$\tilde{\alpha}_k^{(i,j)} \leftarrow \frac{1}{\tilde{W}_k^{(i,\ell)}} \sum_{\jmath \in L} W_k^{(i,\jmath)} \alpha_k^{(i,j)}$
$\tilde{\beta}_k^{(i,j)} \leftarrow \frac{1}{\tilde{W}_k^{(i,\ell)}} \sum_{\jmath \in L} W_k^{(i,\jmath)} \beta_k^{(i,j)}$
$I \leftarrow I/L$
until $I = \emptyset$
If $\ell > J_{max}^{(i)}$ then replace $\left\{\tilde{W}_k^{(i,j)}, \tilde{m}_k^{(i,j)}, \tilde{P}_k^{(i,j)}, \tilde{\alpha}_k^{(i,j)}, \tilde{\beta}_k^{(i,j)}\right\}_{j=1}^{\ell}$ by those of the $J_{max}^{(i)}$ proposed posterior components with largest weights.
output: $\left\{\tilde{W}_k^{(i,j)}, \tilde{m}_k^{(i,j)}, \tilde{P}_k^{(i,j)}, \tilde{\alpha}_k^{(i,j)}, \tilde{\beta}_k^{(i,j)}\right\}_{j=1}^{\ell}$

for detection profile. The real RCS values will be used to the function of probability density (pdf)' prediction for all angles which summarized in Table 2. Fig. 2 shown the function of cumulative density (CDF) for difference statistical distribution models. In the recent multi-Bernoulli algorithms, the variance of measurement is assumed constant value. However, in our case, this assumption is not accurate due to fluctuation of RCS values from state-to-state. Therefore, in this paper we present a novel closed solution of Cubature Kalman-Variational Bayesian-multi-Bernoulli-TBD filter by using the proposed posterior approximation based on the accurate form of the variance of measurement. The accurate formal of variance of measurement ($\boldsymbol{R}$) depending on fluctuate RCS (σ_{drone}) and drone target state (x) is calculated by

$$\boldsymbol{R}\left(x, \sigma_{Drone}\right) = \frac{c}{8B\sqrt{\frac{M.\sigma_{Drone}}{\left((x_t - x_r)^2 + (y_t - y_r)^2\right)^2}}} \tag{40}$$

where (x_r, y_r) and (x_t, y_t) are the states of radar system and target respectively. B and c are waveform bandwidth and speed of light respectively. While M is a suitable constant depending on many parameters (e.g., signal wavelength, transmitter power, transmitter gain, noise figure, etc.). Note that R and probability of detection (a) for real drones are hidden to the algorithms. Therefore, the rows data are simulated related to the state dependent for each model of drone as given in Table 2.

Table 2
Micro-Drone types with measurements variances and average RCS.

Number	Type of micro-drones	RCS (dBsm)	Variances of measurement (m)
1	Phantom 3	−20.5	11 m–7 m
2	Inspire 1	−14.5	7.5 m–4 m
3	Hexacopter	−7.5	4.5 m–1 m

6.2. Performance evaluation

We can evaluate performance of our filter with drone's miss-distance by using the Optimal Subpattern assignment (OSPA). The error between true state and estimated state is performed of any filter. We can use the OSPA metric due to it jointly captures differences in cardinality and individual elements between two finite sets [27]. The OSPA metric $\overline{\mathrm{d}}_{\mathrm{p}}^{(\mathrm{c})}$ is defined as follows. Let $\mathrm{d}^{(\mathrm{c})}(\mathrm{x}, \mathrm{y}) := \min(\mathrm{c}, \|\mathrm{x} - \mathrm{y}\|)$ for $\mathrm{x}, \mathrm{y} \in \mathfrak{X}$, and π_{k} denote the set of permutations on $\{1, 2, \ldots, \mathrm{k}\}$ for any positive integer k. Then, for $\mathrm{p} \geq 1$, $\mathrm{c} > 0$, and $\mathrm{X} = \{\mathrm{x}_1, \ldots, \mathrm{x}_{\mathrm{m}}\}$ and $\mathrm{Y} = \{\mathrm{y}_1, \ldots, \mathrm{y}_{\mathrm{n}}\}$ in *EuScriptF* ($\mathfrak{X}$), we have

$$\overline{d}_p^{(c)}(X, Y) := \left(\frac{1}{n}\left(\min_{\pi \in \prod_n} \sum_{i=1}^{m} d^{(c)}\left(x_i, y_{\pi(i)}\right)^p + c^p(n - m)\right)\right)^{\frac{1}{p}} \tag{41}$$

if $\leq n$, while $\overline{d}_p^{(c)}(X, Y) := \overline{d}_p^{(c)}(Y, X)$ if $m > n$; and $\overline{d}_p^{(c)}(X, Y) := \overline{d}_p^{(c)}(Y, X) = 0$ if $m = n = 0$. This distance is interpreted by pth order per-target error, comprising pth order per-target localization error and pth order per-target cardinality error. The order parameter p determines the sensitivity to outliers, and the cut-off parameter c determines relative weighting of the penalties assigned to cardinality and localization errors. The OSPA metric is also easily computable, for full details see [27].

6.3. Simulation results

In order to test the results of the proposed Cubature Kalman-variational Bayesian (VB)- multi-Bernoulli (CBMeMBer)-TBD filter described above, the CK-GIGM-MB-TBD implementation is demonstrated using the simulation scenario which described in the following, then comparing with VB-CBMeMBer, and CBMeMBer-TBD filters. Assume a 2D scenario space of size 45 m in each dimension. The scenario consists of four drones disappearing and emerging successively as shown in Fig. 3. The image samples from a simulated scenario at the time k = 2, 9, 14, 18 s is shown in Fig. 4. The drones appeared at the pointed positions, but we cannot distinguish it from the heavy noise. Specifically, the dynamical model is non-linear transformation with additive Gaussian noise. The drone target state $\left[A_k, R_k, p_{x,k}, \dot{p}_{x,k}, p_{y,k}, \dot{p}_{y,k}, w_k\right]^T$ comprises the unknown A_k, and variances of measurement $\boldsymbol{R}_k$, state vector of range and speed $\left[p_{x,k}, \dot{p}_{x,k}, p_{y,k}, \dot{p}_{y,k}\right]^T$, the turn rate $\mathrm{w_k}$. The drone target motions are modelled by a nonlinear

(a) Phantom3 (DJI) (b) Inspire 1(DJI) (c) Hexacopter (DJI S900)

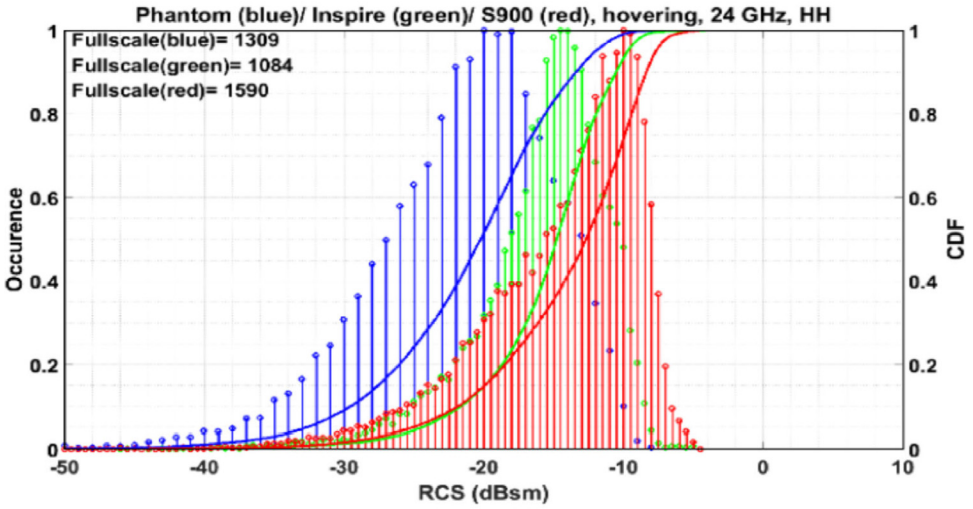

Fig. 2. Geometry model of drones with different size; the histograms of RCS and CDF plots at 24 GHz [12].

constant turn model given by

$$\boldsymbol{x}_{k,\ell} = \Phi_k\left(w_{k-1,\ell}\right)\boldsymbol{x}_{k-1,\ell} + Gw_{k-1,\ell}, \quad w_{k,\ell} = w_{k-1,\ell} + \Delta u_{k-1,\ell} \tag{42}$$

where

$$\Phi_k(w) = \begin{bmatrix} 1 & \frac{\sin w\Delta}{w} & 0 & -\frac{1-\cos w\Delta}{w} \\ 0 & \cos w\Delta & 0 & -\sin w\Delta \\ 0 & \frac{1-\cos w\Delta}{w} & 1 & \frac{\sin w\Delta}{w} \\ 0 & \sin w\Delta & 0 & \cos w\Delta \end{bmatrix},$$

$$G = \begin{bmatrix} \frac{\Delta^2}{2} & 0 \\ \Delta & 0 \\ 0 & \frac{\Delta^2}{2} \\ 0 & \Delta \end{bmatrix} \tag{43}$$

where $\Delta = 1$ s is the sampling period, $w_k \sim \mathcal{N}\left(.; 0, \sigma_w^2 I\right)$, $\sigma_w = 0.1$ m/s^2 is the process noise, $u_k \sim \mathcal{N}\left(.; 0, \sigma_u^2\right)$ and $\sigma_u = (\pi/90)$ rad/s. The probability of survival is $p_{S,k} = 0.99$. The simulation uses the maximum of mixers as $J_{max} = 1000$. We will use $N = 1000$ birth particles and $N = 1000$ continuing particles to simulate the SMC-MB-TBD algorithm. The drone birth Cubature Kalman-Variational Bayesian-CBMeMBer-TBD process is a RFS Cubature Kalman-multi-Bernoulli with distribution

$$\pi_{\Gamma,k} = \left\{\left(r_{\Gamma,k}^{(i)}, p_{\Gamma,k}^{(i)}\right)\right\}_{i=1}^{4}, r_{\Gamma,k}^{(1)} = r_{\Gamma,k}^{(2)} = r_{\Gamma,k}^{(3)} = r_{\Gamma,k}^{(4)} = 0.02$$

$$P_{\Gamma,k}^{(i)}(x, \boldsymbol{R}) = w_{\Gamma,k}^{(i)} N\left(x; m_{\Gamma,k}^{(i)}, p_{\Gamma,k}^{(i)}\right) \times \prod_{l=1}^{d=3} \text{Inv} - \text{Gamma}\left(\left(\sigma_{\Gamma,k,l}^{(i)}\right)^2; \alpha_{\Gamma,k,l}^{(i)}, \beta_{\Gamma,k,l}^{(i)}\right) \tag{44}$$

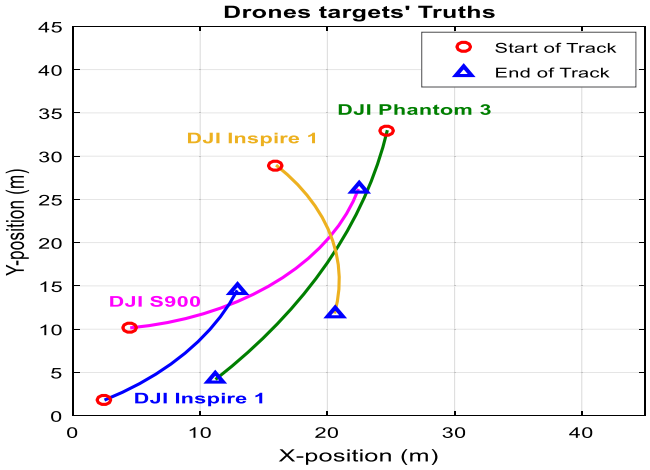

Fig. 3. The four drones' trajectories in x – y plane, start/end denoted by O/△.

where $m_{\Gamma,k}^{(1)} = [25, 0, 35, -1, \pi/360]^T$, $m_{\Gamma,k}^{(2)} = [13, 1, 10, 0, \pi/360]^T$, $m_{\Gamma,k}^{(3)} = [1, 1.5, 1, 0.5, \pi/360]^T$, $m_{\Gamma,k}^{(4)} = [15, 1, 30, -1, \pi/360]^T$, $p_{\Gamma,k} = \text{diag}\left([0.5, 0.5, 0.5, 0.5, 6\,(\pi/180)]^T\right)^2$, $w_{\Gamma,k}^{(i)} = 0.2$, $\alpha_{\Gamma,k,l}^{(i)} = \beta_{\Gamma,k,l}^{(i)} = 1$, $\boldsymbol{R}_k^{(i)} = \text{diag}\,[1111] = \text{diag}\left[\beta_{k,1}^{(i)}/\alpha_{k,1}^{(i)}, \beta_{k,2}^{(i)}/\alpha_{k,2}^{(i)}, \beta_{k,3}^{(i)}/\alpha_{k,3}^{(i)}, \beta_{k,4}^{(i)}/\alpha_{k,4}^{(i)}\right]$.

The image observation is 45 pix × 45 pix array, giving each cell side lengths of $\Delta_x = \Delta_x = 1$ m. Since the observation array is an image, the index of array treats as an ordered integers' pair $i = (a, b)$, where $1 \le a, b \le 45$. Let us consider that $\boldsymbol{R}_k$ hidden for all algorithms, blurring factor $\sigma_h^2 = 1$, and $(p_{x,k}, p_{y,k})$ is the state position. The observation of image is shown in Fig. 4. The merging threshold denoted by $T_{merge} = 0.75$ times the pixel width. Tracks

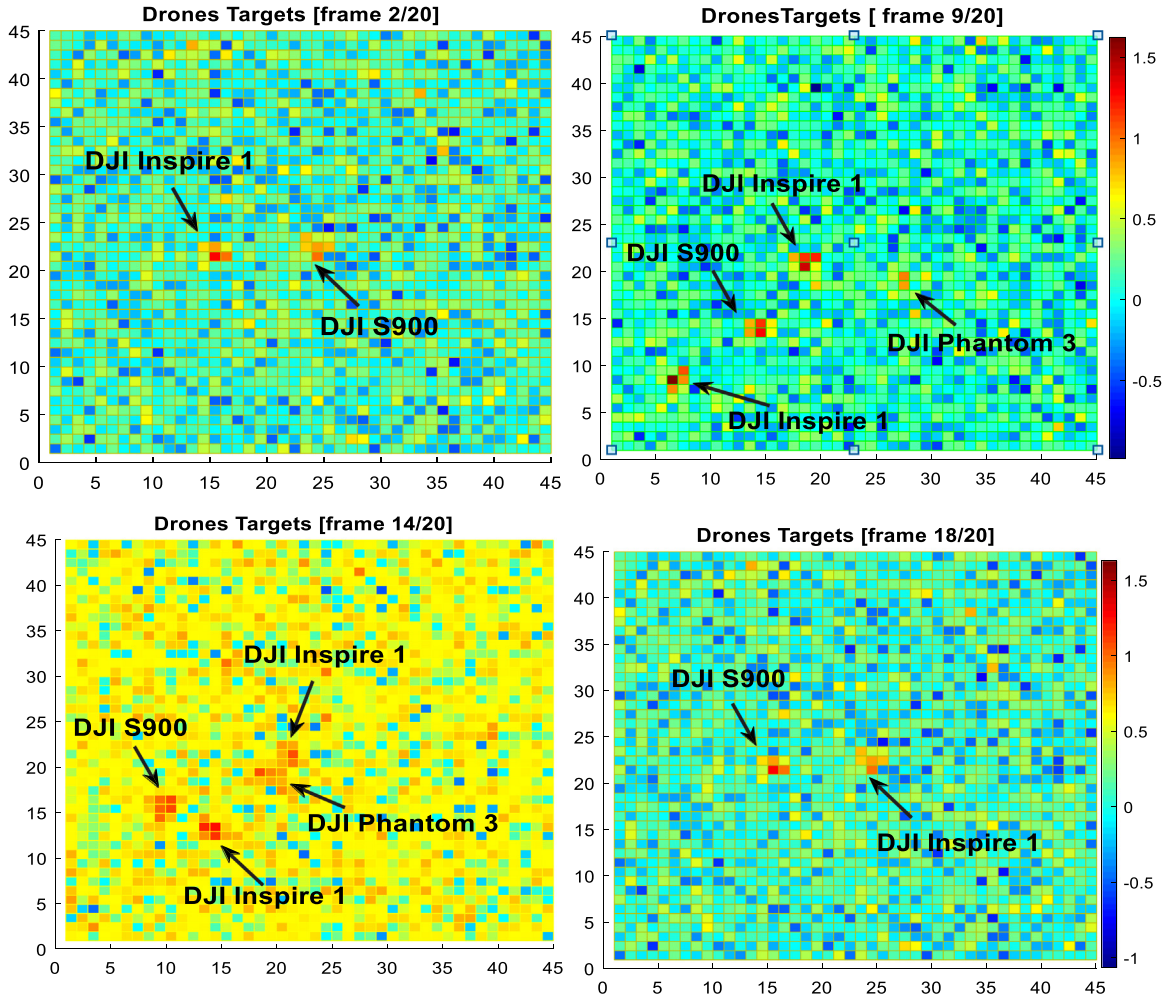

Fig. 4. The frames of measurement at different times.

with $r < 10^{-2}$ are cancelled then the tracks maximum will be $T_{max} = 100$. Since no prior information was available on the measurement noise variance, thus the initial parameters of inverse Gamma distribution are set as $\alpha_0 = \beta_0 = 1$. In VB-CBMeMBer [20], CBMeMBer-TBD [14] filters which are used in the simulation, these filters have the same parameters on the posterior distribution. The OSPA distance (for $p = 1$ and $c = 30$) are shown for all algorithms. The selected ρ_l is very difficult, because of the changing of estimated noise. Therefore the results will be improved when $\rho_l = 0.95$. Also we can consider $\boldsymbol{R} = 5$ m for CBMeMBer-TBD [4], and $a = 0.7$ for VB-CBMeMBer [20] for all targets. The results of simulation are implemented by 200 MC runs and shown in Figs. 4–8. Fig. 4 shows the four drones' coordinates against time that are processed in a one run by all algorithms with unknown $\boldsymbol{R}$. As shown in Fig. 4, in case of high SNR (k = 2, 9, 18 s) and low SNR (k = 14 s), the proposed CK-VB-CBMeMBer-TBD filter can obtain detailed drones' information. As we shown in Fig. 5, our algorithm has a new estimation for the fluctuated $\boldsymbol{R}$ with good performance than other filters. The results show that the Cubature Kalman-VB-CBMeMBer-TBD filter is more accurate performance of tracking. But, the other algorithms have drops of performance' tracking because of the unknown a for VB-CBMeMBer filter, and unknown $\boldsymbol{R}$ for CBMeMBer-TBD algorithm. Based on the simulation results, our algorithm has the ability to estimate the trajectories of all targets. As shown in Fig. 6, our algorithm has an easy handling crossing of Inspire 1 and Phantom 3 at time t = 10, and Hexacopter and Inspire1 at time t = 13. In addition, the estimated cardinality of drones by all algorithms is shown in Fig. 6. In Fig. 7, we shown that the estimated RMSEs. As shown the Cubature Kalman(CK)-VB-CBMeMBer-TBD algorithm has an accurate estimating the drones number than the other algorithms with unknown profile of detection. This is because of the unknown $\boldsymbol{R}$ is jointing estimation with TBD scheme by our filter. In addition, the results performance of VB-CBMeMBer and CBMeMBer-TBD filters have a degradation with σ parameter. This is because of assuming that the constant value $\sigma = 5$ m for CBMeMBer-TBD and since it does not deviate from the true value. While, assumed value a = 0.7 for VB-CBMeMBer is also inaccurate due to not deviate from the true value. Fig. 8 shows the OSPA comparison in three filters, and it is shown that proposed algorithm outperforms SMC-CBMeMBer-TBD and VB-CBMeMBer algorithms. This is because of the proposed method allows more reliable extraction of state estimates than other two methods. In the all filters, the estimated states are the means of posterior densities. Fig. 9 show average RMSEs and OSPA under different SNR (dB). It is obvious that tracking accuracy of three algorithms increase on SNR. In addition, the accuracy of CK-VB-CBMeMBer-TBD algorithm is always higher than VB-CBMeMBer and SMC-CBMeMBer-TBD algorithms.

The average running time for each filter iteration (a one prediction and update step) in seconds is reported in Table 3. First, note that the SMC-MB-TBD implementations take significantly more time to compute than the CK-GIGM-MB-TBD and VB-MB-TBD implementations, which is expected. It should also be noted that, as expected, the CK-GIGM-MB-TBD implementation require

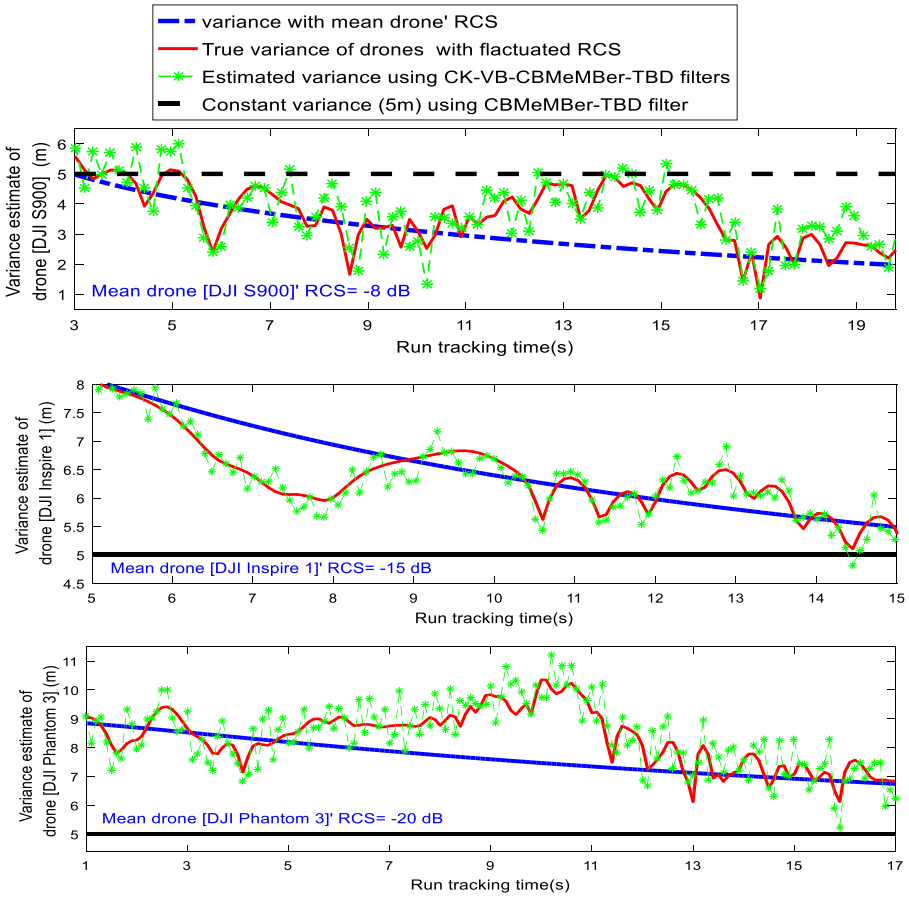

Fig. 5. The estimation of the variances of measurement at different times.

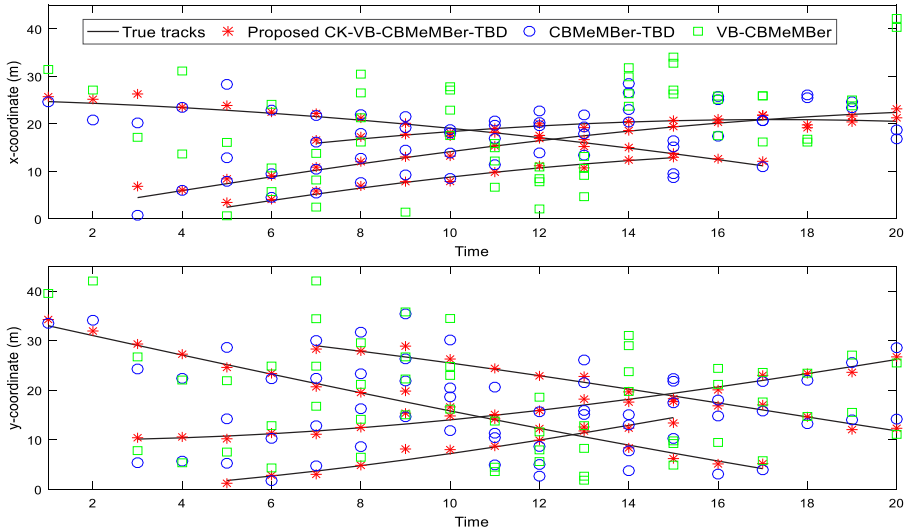

Fig. 6. The tracking results in x and y directions at different times.

more computational time than their respective one model counterparts. However, the increase in computational time is minimal for each implementation. The real-time performance of the CK-GIGM-MB-TBD filter is superior to the VB-MB-TBD filter, because the VB-MB-TBD filter only needs $|\boldsymbol{Z}_k|$ to approximate the probability density, while the CK-GIGM-MB-TBD filter needs 2_j sigma points. The real-time performance of the SMC-MB-TBD filter is the worst, because the SMC-MB-TBD filtering algorithm needs a large number of the particles (N^2). From this experiment, we found the average running times were 98.63 s for SMC-MB-TBD filter, 37.54 s for CK-GIGM-MB-TBD filter and 25.34 s for GIGM-MB-TBD filter. That is, the proposed CK-GIGM-MB-TBD filter has the best real-time performance after VB-MB-TBD. The real-time performance of the SMC-MB-TBD filter is the worst, because the SMC-MB-TBD filtering algorithm needs a large number of the particles. Therefore, in view of both the filtering performance and the real-time performance, the CK-GIGM-MB-TBD filter is an attractive approach.

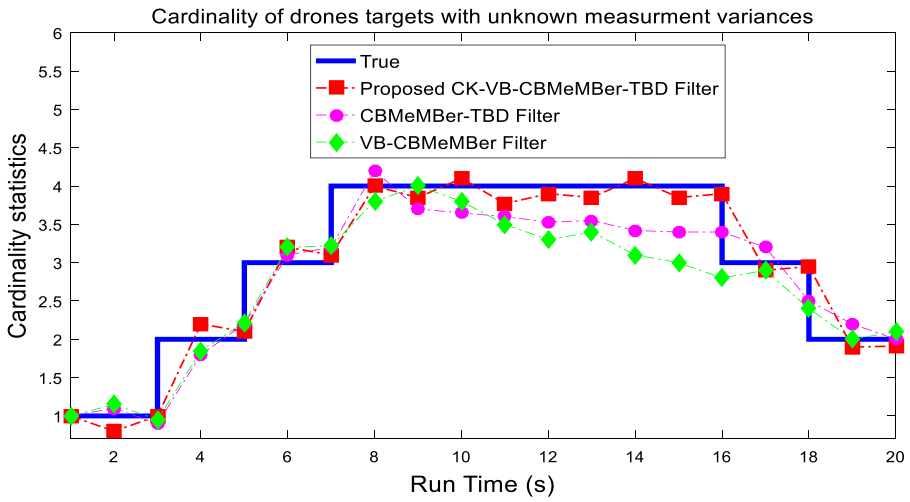

Fig. 7. The cardinality estimation at different times.

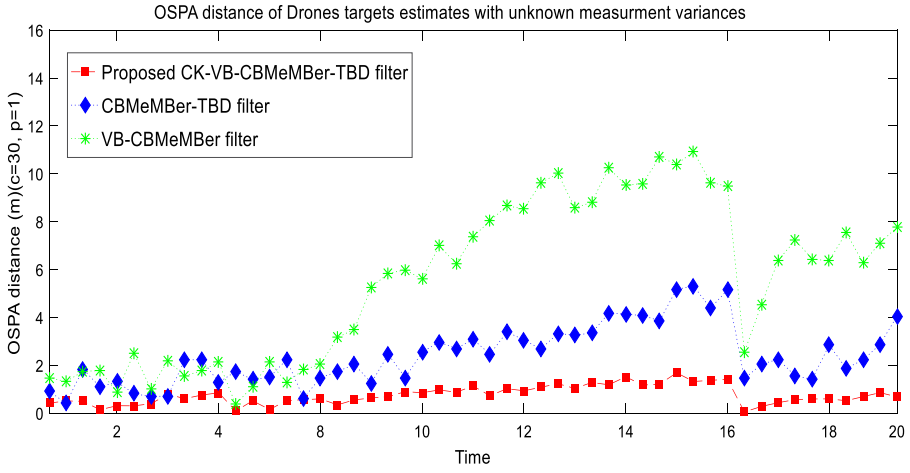

Fig. 8. The average OSPA distance statistic estimation.

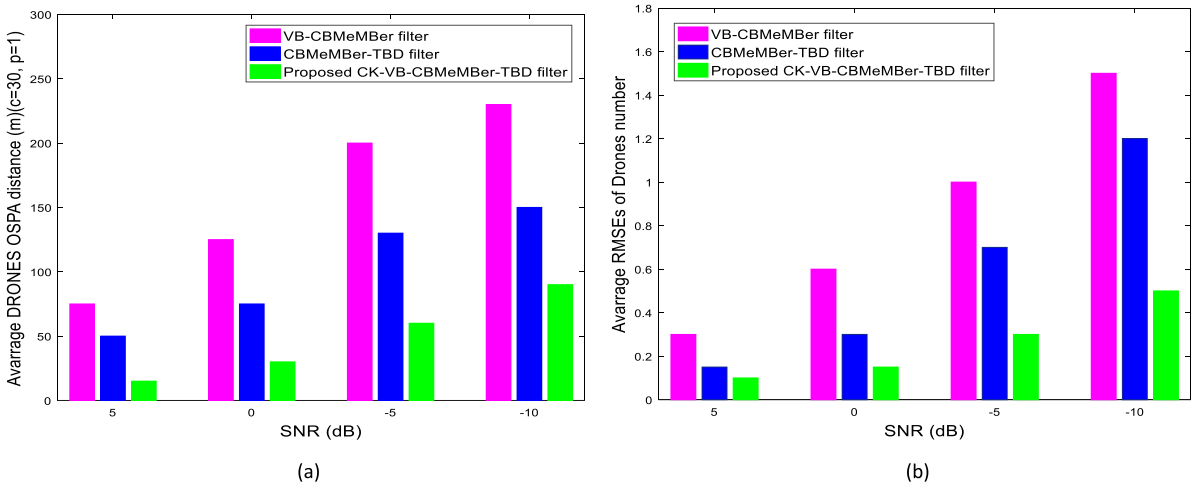

Fig. 9. Average OSPA distances and average RMSE of cardinality estimate against SNR (dB). (a) Average OSPA distances (b) Average RMSE of cardinality estimate.

7. Discussion and conclusion

In this paper, we consider the proposed robust Cubature Kalman (CK)-MB-TBD filter for tracking of multiple drone targets. The MB-TBD algorithm has been widely used to handle the non-linear models for small target tracking with good performance. This filter implemented by the Sequential Monte Carlo (SMC) method. However, this implementation has the problem of larger

Table 3
Average running time for single Monte Carlo, s.

Sequential Monte Carlo (SMC)-MB-TBD	Cubature Kalman (CK)-GIGM-MB-TBD	Variational Bayesian (VB)-MB-TBD
98.63	37.54	25.34

computation complexity and only adapted slowly to the variances of measurement. The filtering accuracy of this filter is the worst. This is because the number of particles for each tracks is not enough. This will limit the real-time performance of the MB-TBD filtering. To solve this problem, we summarize the contributions of this paper as

- To solve this problem, we proposed a novel Cubature Kalman-multi-Bernoulli-TBD filter. The proposed algorithm employs a third-degree spherical-radical cubature rule. This filter is more accurate rather than the SMC-multi-Bernoulli-TBD filter and more principled in mathematical terms. This is the first time to use this Cubature Kalman-multi-Bernoulli filter for TBD approach. However, the proposed algorithm has implemented with fixed and known variances of measurement. Since the variances of measurement are unknown in a real tracking scenario for small targets like drones.
- To solve the problem of unknown variances of measurement due to the fluctuation of RCS. We improve the proposed algorithm to be suitable for tracking small objects with unknown variances of measurement. This improvement has applied with the approximated variational Bayesian approach to update the object state with unknown variances of measurement. This is the first time to use the proof of concept of this robust method for Cubature Kalman-multi-Bernoulli filter and TBD approach. Therefore, we propose a robust approximated variational Bayesian jointing with Cubature Kalman-multi-Bernoulli-TBD filter. The proposed algorithm has less computational burden comparing to SMC-multi-Bernoulli-TBD filter.

The CK-VB-MB-TBD process is also approximated by CK-GIGM-MB-TBD implementation of non-linear Scenario. Thus, there are the ability of calculate the non-linear kinematic state of drone target hybrid with unknown variances of measurement. The results confirm the effectiveness and robustness of the proposed algorithm.

Declaration of competing interest

The authors declare that they have no known competing financial interests or personal relationships that could have appeared to influence the work reported in this paper.

Appendix A

The Legendre polynomial iteration to reconstruct the pdf [7–9] is obtained in Appendix A.

$$p\left(\Upsilon_k|\overline{\Upsilon}\right) = p_d\left(\sigma|\overline{\sigma}\right) = \frac{1}{\sigma_L} p_d\left(\frac{\sigma-\overline{\sigma}}{\sigma_L}\right) = \frac{1}{\sigma_L}\sum_{n=0}^{\infty} a_n L_n\left(\frac{\sigma-\overline{\sigma}}{\sigma_L}\right) \tag{A.1}$$

where $\sigma_L = \sigma_{max} - \sigma_{min}$, L_n is the expression of Legendre polynomial given by

$$L_n\left(\frac{\sigma-\overline{\sigma}}{\sigma_L}\right) = \sum_{k=0}^{[n/2]} \frac{(-1)^k (2n-2k)!}{2^n k!\,(n-k)!\,(n-2k)!}\left(\frac{\sigma-\overline{\sigma}}{\sigma_L}\right)^{n-2k} \tag{A.2}$$

a_n refer to coefficients determined by the kth central moments of σ and $M_\sigma^{(k)}$ as

$$a_n = \frac{2n+1}{2}\sum_{k=0}^{[n/2]} \frac{(-1)^k (2n-2k)!}{2^n k!\,(n-k)!\,(n-2k)!}\frac{M_\sigma^{(n-2k)}}{{\sigma_L}^{n-2k}} \tag{A.3}$$

where

$$M_\sigma^{(k)} = \int_{-\infty}^{+\infty} (\sigma-\overline{\sigma})^k p_\sigma(\sigma)\, d\sigma, (k = 0, 1, 2, \ldots) \tag{A.4}$$

Appendix B

The iteration The CK-GIGM-MB-TBD updating following as:

$$\boldsymbol{R}_k^{(i,j)(n)} = diag\left[\frac{\beta_{k,1}^{(i,j)(n)}}{\alpha_{k,1}^{(i,j)}}, \frac{\beta_{k,2}^{(i,j)(n)}}{\alpha_{k,2}^{(i,j)}}, \ldots, \frac{\beta_{k,d}^{(i,j)(n)}}{\alpha_{k,d}^{(i,j)}}\right] \tag{B.1}$$

$$e_k^{(i)(n)}(\boldsymbol{R}, z) = \sum_{j=1}^{J_{k/k-1}^{(i)}} W_{k|k-1}^{(i,j)} N\left(z; \boldsymbol{\eta}_{k|k-1}^{(i,j)}, \mathbb{S}_{k|k-1}^{(i,j)} + \boldsymbol{R}_k^{(i,j)(n)}\right) \tag{B.2}$$

$$\boldsymbol{\eta}_{k|k-1}^{(i,j)} = \frac{1}{2\jmath}\sum_{\ell=1}^{2\jmath} \boldsymbol{h}_k\left(\chi_{k|k-1}^{(i,j)}(\ell)\right) \tag{B.3}$$

$$\chi_{k|k-1}^{(i,j)}(\ell) = m_{k|k-1}^{(i,j)} + \mathbb{C}_{k|k-1}^{(i,j)}\xi(\ell) \tag{B.4}$$

$$\mathbb{C}_{k|k-1}^{(i,j)} = \mathbf{chol}\left[P_{k|k-1}^{(i,j)}\right]^T \tag{B.5}$$

$$\mathbb{S}_{k|k-1}^{(i,j)} = \frac{1}{2\jmath}\sum_{\ell=1}^{2\jmath}\left(\boldsymbol{\eta}_{k|k-1}^{(i,j)} - \boldsymbol{h}_k\left(\chi_{k|k-1}^{(i,j)}(\ell)\right)\right) \times \left(\boldsymbol{\eta}_{k|k-1}^{(i,j)} - \boldsymbol{h}_k\left(\chi_{k|k-1}^{(i,j)}(\ell)\right)\right)^T \tag{B.6}$$

$$\boldsymbol{G}_k^{(i,j)(n)} = \frac{1}{2\jmath}\sum_{\ell=1}^{2\jmath}\left(m_{k|k-1}^{(i,j)} - \chi_{k|k-1}^{(i,j)}(\ell)\right) \times \left(\boldsymbol{\eta}_{k|k-1}^{(i,j)} - \boldsymbol{h}_k\left(\chi_{k|k-1}^{(i,j)}(\ell)\right)\right)^T \tag{B.7}$$

$$\boldsymbol{K}_k^{(i,j)(n)} = \boldsymbol{G}_k^{(i,j)(n)}\left[\mathbb{S}_{k|k-1}^{(i,j)} + \boldsymbol{R}_k^{(i,j)(n)}\right]^{-1} \tag{B.8}$$

$$m_k^{(i,j)(n)}(z) = m_{k|k-1}^{(i,j)} + \boldsymbol{K}_k^{(i,j)(n)}\left[z - \boldsymbol{\eta}_{k|k-1}^{(i,j)}\right] \tag{B.9}$$

$$P_k^{(i,j)(n)} = P_{k|k-1}^{(i,j)} - \boldsymbol{K}_k^{(i,j)(n)}\mathbb{S}_{k|k-1}^{(i,j)}\left[\boldsymbol{K}_k^{(i,j)(n)}\right]^T \tag{B.10}$$

$$W_k^{(i,j)(n)}(\boldsymbol{x}, \boldsymbol{R}; z) = W_{k/k-1}^{(i,j)} N\left(z; \boldsymbol{\eta}_{k|k-1}^{(i,j)}, \mathbb{S}_{k|k-1}^{(i,j)} + \boldsymbol{R}_k^{(i,j)(n)}\right) \tag{B.11}$$

$$\beta_{k,l}^{(i,j)(n+1)} = \beta_{k,l}^{(i,j)(n)} + \frac{1}{2}\left(z - \boldsymbol{h}_k m_k^{(i,j)(n)}\right)_i^2 + \frac{1}{2}\left(\boldsymbol{h}_k P_k^{(i,j)(n)}(\boldsymbol{h}_k)^T\right)_{ii} \tag{B.12}$$

where $n \in [1, N]$, N known by the maximum iterations number. If the state estimation pass $\left\|m_k^{(i,j)(n)} - m_k^{(i,j)(n-1)}\right\| < \varepsilon$, then the iteration end, and the estimated parameters are calculated as $W_k^{(i,j)} = W_k^{(i,j)(n)}$, $m_k^{(i,j)} = m_k^{(i,j)(n)}$, $p_k^{(i,j)} = p_k^{(i,j)(n)}$ and $\beta_{k,l}^{(i,j)} = \beta_{k,l}^{(i,j)(n)}$. Otherwise, the iterations will be continued from (B.1)–(B.12).

References

[1] Ouyang C, Ji H, Li C. Improved multi-target multi-Bernoulli filter. IET Radar Sonar Navig 2012;6(6):458–64.
[2] Ristic B, Vo B-T, Vo B-N, Farina A. A tutorial on Bernoulli filters: Theory, implementation and applications. IEEE Trans Signal Process 2013;61(13):3406–30.
[3] Vo B-N, Vo B-T, Cantoni A. The cardinality balanced multi-target multi-bernoulli filter and its implementations. IEEE Trans Signal Process 2009;57(2):409–23.

[4] Vo B-N, Vo B-T, Hoseinnezhad R, Mahler R. Robust multi-Bernoulli filtering. IEEE J Sel Top Signal Process 2013;7(3):399–409.
[5] Rahman S, Duncan R. In-flight RCS measurements of drones and birds at K-band and W-band. IET Radar Sonar Navig 2019;13(2):300–9.
[6] Patel1 J, Fioranelli F, Anderson D. Review of radar classification and RCS characterisation techniques for small UAVs or drones. IET Radar Sonar Navig 2018;12(9):911–9.
[7] Salim IM, Barbary M, AbdEl-azeem MH. Novel Bayesian track-before-detection for drones based VB-multi-Bernoulli filter and a GIGM implementation. Radioengineering 2020;29(2):397–404.
[8] Zong P, Barbary M. Improved multi-Bernoulli filter for extended stealth targets tracking based on sub-random matrices. IEEE Sens J 2016;16(5):1428–47.
[9] Barbary M, Zong P. Novel anti-stealth on Sub-Nyquist scattering Wave deception Jammer with Stratospheric Balloon-borne Bistatic Radar using KA-STAP-FTRAB Algorithm. IEEE Sens J 2015;15(11):6437–53.
[10] Quevedo A, Urzaiz F, Menoyo J, López A. Drone detection and radar-cross-section measurements by RAD-DAR. IET Radar Sonar Navig 2019. (Accepted on 17th 2019).
[11] Yang J, Ji H, Ge H. Multi-model particle cardinality-balanced multi-target multi-Bernoulli algorithm for multiple manoeuvring target tracking. IET Radar Sonar Navig 2013;7(2):101–12.
[12] Dunne D, Kirubarajan T. Multiple model multi-Bernoulli filters for manoeuvering targets. IEEE Trans Aerosp Electron Syst 2013;49(4):2679–92.
[13] Doucet A, Freitas N, Gordon N. Sequential Monte Carlo methods in practice. New York: Springer; 2001.
[14] Vo B-N, Vo B-T, Pham N, Suter D. Joint detection and estimation of multiple objects from image observations. IEEE Trans Signal Process 2010;58(10):5129–41.
[15] Vo BT, See CM, Ma N, Ng WT. Multi-sensor joint detection and tracking with Bernoulli filter. IEEE Trans Aerosp Electron Syst 2012;48(2):1385–402.
[16] Yang J, Ge H. Adaptive probability hypothesis density filter based on variational Bayesian approximation for multi-target tracking. IET Radar Sonar Navig 2013;7(9):959–67.
[17] Wu X, Huang G, Gao J. Adaptive noise variance identification for probability hypothesis density-based multi-target filter by variational Bayesian approximations. IET Radar Sonar Navig 2013;7(8):895–903.
[18] Sarkkak S, Nummenmaa A. Recursive noise adaptive kalman filtering by variational Bayesian approximations. IEEE Trans Automat Control 2009;54(3):596–600.
[19] Bo G, Heng T, Long L. Multi-sensor centralized fusion without measurement noise covariance by variational Bayesian approximation. IEEE Trans Aerosp Electron Syst 2011;47(1):718–27.
[20] Yang J, Ge H. An improved multi-target tracking algorithm based on CBMeMBer filter and variational Bayesian approximation. Signal Process 2013;93:2510–5.
[21] Arasaratnam I, Haykin S. Cubature Kalman filters. IEEE Trans Automat Control 2009;54(6):1254–69.
[22] M. Liu T, Jiang X, Wang, Zhang S. Performance comparison of several nonlinear multi-Bernoulli filters for multi-target filtering. In: 17th international conference on information fusion (FUSION). 2014.
[23] Haihuan WL, Xiaoyong M, Long. Adaptive cardinality balanced multi-target multi-Bernoulli filter based on cubature Kalman. J Eng 2019;2019(21):7667–71.
[24] Bocquel M. Random finite sets in multi-target tracking - efficient sequential MCMC implementation (Ph.D. thesis), Enschede: Centre for Telematics and Information Technology (CTIT); 2013.
[25] Paolo P, Martin P. Improving extent estimation of extended targets with Track-before-Detect. In: 19thinternational conference on information fusion (FUSION). 2016.
[26] Malher R, Vo B-N, Vo B-T. CPHD with unknown clutter rate and detection profile. IEEE Trans Signal Process 2011;59(8):3497–513.
[27] Schuhmacher D, Vo B-N, Vo B-T. A consistent metric for performance evaluation of multi-object filters. IEEE Trans Signal Process 2008;56(8):3447–57.